Chapter 8
How to Utilise the Knowledge of Causal Responses?

Pertti Hari, Mikko Havimo, Heljä-Sisko Helmisaari, Liisa Kulmala, Eero Nikinmaa, Timo Vesala, Jouni Räisänen, Tuukka Petäjä, Erkki Siivola, Heikki Tuomenvirta, Jaana Bäck, John Grace, Federico Magnani, Twan van Noije, Jukka Pumpanen, David Stevenson, Markku Kulmala, Sampo Smolander, Ilona Riipinen, and Miikka dal Maso

Contents

Abstract Our physical and physiological theory provides causal explanations of various phenomena in forests. This causal nature of the theory enables versatile applications in forestry and in the research of the interactions between climate change and forests. We treat the effects of thinnings and whole-tree harvesting on wood production and the responses of forest ecosystem to nitrogen deposition in more detail. The forests react to the increasing CO_2 concentration and also to temperature increase generating feedbacks from forests to climate change. The changes in the carbon storages in forest ecosystems and in the emission of volatile organic compounds are evidently the most important feedbacks from forest ecosystems to the climate change.

P. Hari (✉)
Department of Forest Sciences, University of Helsinki, P.O. Box 27, 00014 University of Helsinki, Helsinki, Finland
e-mail: pertti.hari@helsinki.fi

P. Hari et al. (eds.), *Physical and Physiological Forest Ecology*,
DOI 10.1007/978-94-007-5603-8_8,

Keywords Forestry • Thinning • Whole-tree harvesting • Climate change • Response of forest ecosystem • Feedback to climate change

8.1 Introduction

Our theories provide causal explanations of many phenomena in forest ecosystems based on metabolism of living organisms, on transport of material and energy and on structural regularities developed during evolution. These causal explanations enable exploration of a wide range of applications in forestry and facilitate research on the effects of climate change on forests.

The extinction of light in the canopy conveys the principal interaction between trees. This opens a fruitful way to explain the growth of dominating and suppressed trees in a stand and also the effect of stand density on growth of individual trees. Nitrogen in many chemical forms within trees is removed from the stand by the practice of whole-tree harvesting, thus reducing the amount of reactive nitrogen in the remaining stand and reducing the tree growth in the stand. Anthropogenic nitrogen deposition increases the amount of reactive nitrogen in forest ecosystems resulting in a slow increase in the fertility of the sites.

The present climate change effects on processes in forest ecosystems, that is, increasing CO_2, enhance photosynthesis while increasing temperature accelerates decomposition of proteins in the soil, and at the same time, nitrogen deposition increases reactive nitrogen in forests. All these changes increase forest growth. The changes in the processes are also reflected into the feedbacks from forests to climate change since they affect the atmospheric CO_2 and aerosol concentrations.

8.2 Applications to Forestry

Pertti Hari, Mikko Havimo, Heljä-Sisko Helmisaari, Liisa Kulmala, and Eero Nikinmaa

8.2.1 The Effect of Thinnings on Wood Production

The influence of stand density on timber dimensions and production is one of the main questions to optimise in forest management. The large but fluctuating price difference between that of sawn wood and pulpwood guarantees that the question

P. Hari (✉)
Department of Forest Sciences, University of Helsinki, P.O. Box 27, 00014 University of Helsinki, Helsinki, Finland
e-mail: pertti.hari@helsinki.fi

remains a valid driver for management decisions. The increasing use of wood as a renewable source of energy is expanding again the usage and dimensions of forest products, and it is expected that market prices will change. These considerations will also influence optimal management regimes, not to mention the impact that the changing climate will have.

The main approach to study the effects of thinnings on forest growth has been observational, relying on permanent and semipermanent sample plots. Permanent sample plots have been established at varying site fertilities, tree species, species mixtures, etc., and valuable results have been obtained. However, the interpretation of the results is problematic since by necessity the experiments are long-lasting, and during the passage of time, the relevant research questions may well have changed, hence making the results somewhat redundant.

Statistical methods have been the main tool in growth studies, and regression models have been developed to link directly the tree dimensions and stand level variables with growth. These models give rather good predictions of growth in the time span of a couple of decades. The statistical approach has also been used to study the effect of stand density on growth. The idea there is that the stand growth conditions and competition between trees can be described with stand level variables such as dominant height and stand density, and the response of any individual tree would be reflected in its own dimensions. However, there are both theoretical and methodological problems involved, particularly when simulating the influence of actions that drastically alter the stand conditions such as thinning.

Theoretically, it is problematic to explain how stand basal area or any other tree characteristic of tree stems has a causal effect on growth; the observed correlations are only indicators of the connections between the stand dimensions and growth under the specified conditions. The explaining factors in a causal regression model should be independent of each other when the model is used as causal explanation. However, the stand characteristics are strongly correlated. This correlation of the variables can be utilised in the growth analysis under regular conditions, but during thinning, the nature of the correlation changes, and this makes the use of regression models in the analysis of the effects of thinning and initial density on tree growth very problematic. To be able to account for the thinning impacts with regression type analysis, we would need to have a very large set of treatments that would cover the varying initial densities in different ages, treatment strengths and growth responses, which is experimentally costly and requires observations that are very difficult to carry out. Even in this case, we are facing the problem of connections between explaining variables that are problematic for the causal use of the regression model.

In the true causal approach, the growth results from the underlying combination of environmental conditions, the metabolic and structural state of the trees and the different processes leading to tree growth. The interactions between trees reduce the growth of individual trees from what it could be if those trees were grown without competition. The main mechanisms to decrease growth of individual trees are the extinction of light in the canopy and the consequent reduced photosynthesis, especially in the lower parts of the crown, and also the low availability of nitrogen in the soil. When the stand is thinned, then the needles of the remaining trees

receive more light than previously resulting in increased photosynthesis and growth in the remaining trees. In addition, the thinning increases nitrogen availability that contributes to the enhanced growth. These changes also influence the allocation of growth within trees as the time constants for additional light and nitrogen release are different, thus influencing growth allocation between root and shoot growth. Also the improved light climate of the crown influences the allocation of growth between stem and leaves. These causal mechanisms of the effect of thinning on tree growth are built into MicroForest which deals with the carbon and nitrogen fluxes and with the allocation of the obtained resources within the tree. Thus, we can analyse the responses of tree growth to thinning using MicroForest.

8.2.1.1 Simulations

The stand around SMEAR II measuring station (Section 9) is an even-aged and artificially regenerated Scots pine forest. We utilise MicroForest, and we start from the initial state when the seedlings are small, less than 1 m tall, and simulate the stand development for 80 years at varying thinnings. In order to show the potential for management purposes, we treat separately sawn wood and pulpwood.

We used the measured diameters and heights in each size class at the age of 5 years as the initial state of the stand in the simulations. We divided the stand into five size classes, and the shares of the number of stems in the five size classes were 5, 15, 30, 30 and 20% starting from the biggest size class. We used the measured values at SMEAR II as the initial state of the soil organic matter. The number of seedlings in the initial state was 2,000 per ha.

We applied two thinnings from below in the simulations. The thinnings occurred at the ages of 35 and 55 years, a common thinning schedule for Scots pine forest in south Finland. We varied the intensity in both thinnings in such way that the number of remaining trees increased at 5% interval starting from 15 to 100%.

We classified the wood obtained in the thinnings into pulpwood and sawlogs using the commercial minimum dimensions for pulpwood and sawlogs.

8.2.1.2 Results

The thinnings reduce the stand needle mass, especially in the heavy treatments (Fig. 8.1a). The recovery of the needle mass depends both on the thinning intensity and the stand age. If about 50% of the trees in the stand are thinned, the foliage recovers in about 20 years to the value it had before thinning (Fig. 8.1a). In more moderate thinnings, the recovery takes place in about 10 years in the simulations. The annual flux of ammonium ions from soil proteins caused by microbial decomposition, nitrogen deposition and fixation determines the annual amount of proteins synthesised for the growth of new tissues and in this way the growth of needle mass.

The simulated response in photosynthesis is clearly smaller than the reduction in the needle mass. The shading of the remaining trees by neighbouring trees is less

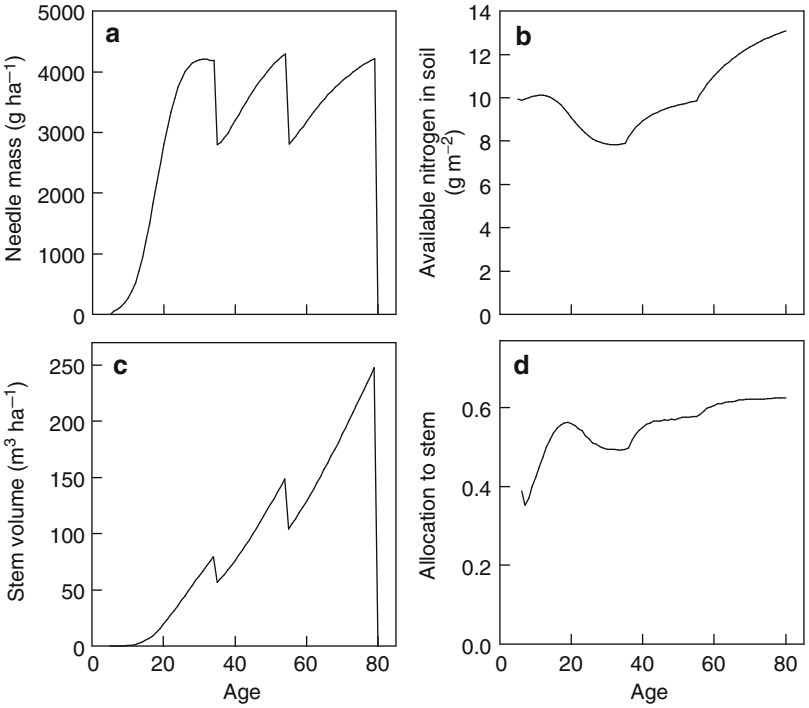

Fig. 8.1 The simulated needle mass (**a**), available nitrogen in the soil (**b**), stand volume (**c**) and allocation to stem (**d**) as function of stand age. Each thinning from below at the age of 35 and 55 years removes 50% of the trees

severe, and so the needles lower in the canopy can photosynthesise more after the thinning than before it. No reduction in the annual amount of photosynthesis was observed immediately after experimental thinning at SMEAR II site in which about 50% of the stem number and about 25% of the stem volume was removed (Vesala et al. 2005). These authors argued that the result was both due to remaining trees and ground vegetation compensating for the decreased foliage and reduction in the root respiration rate associated with lowered biomass.

The thinnings also affected the nitrogen availability in the soil (Fig. 8.1b). When thinnings reduce the simulated needle mass, then the nitrogen uptake of trees is also reduced. The increased growth of ground vegetation is not able to compensate for the reduction in the nitrogen uptake by trees, and the pool of available nitrogen increases slightly. Thus, the thinnings have two effects: increased photosynthetic production and increased nitrogen availability.

The simulated stand volume responded to the thinnings; however, the reduction in volume was clearly smaller than in the number of trees (Fig. 8.1c). This is as expected since the thinnings removed the smaller trees. The volume growth decreased slightly during the first 10 years after thinning, the more as more trees

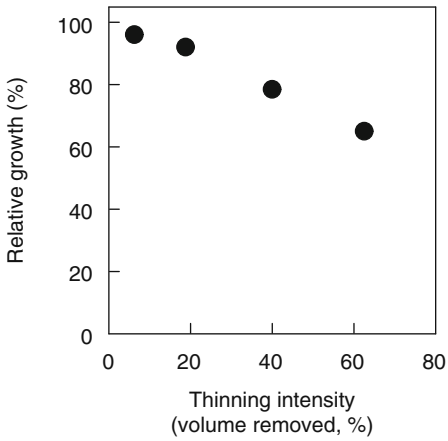

Fig. 8.2 Relative volume growth as function of thinning intensity according to Eriksson and Karlsson (1997)

were removed. After 10–20 years from thinning, the growth recovered completely to the pre-thinning growth rate with exception of the most extreme case of 60% tree removal, in which case the growth was still only about 90% of the pre-thinning value. Thus, although the thinnings reduced the needle mass and the annual photosynthetic production, the trees were able to produce nearly the same amount of wood. The growth immediately after thinning corresponded very closely to observations made in similar age pine stands (Eriksson and Karlsson 1997) (Fig. 8.2). However, the model predicted somewhat better recovery of growth on the long run than was observed.

The allocation of sugars and nitrogen is very demanding task for the biochemical regulation system. The observed regularities in tree structure indicate that trees are able to solve the allocation problem. The thinnings affect allocation in two different ways, the increased nitrogen availability reduces the share of roots and the increasing needle mass per tree in the remaining stand requires more water transport capacity in the stem. The increase in nitrogen availability in soil takes years, and the response of root allocation is also slow. The simulated allocation to stem (Fig. 8.1d) indicates rapid and clear response to the thinnings as we expected from the theoretical argumentation. The increased allocation to stem growth explains the strange result that thinnings reduce annual photosynthetic production, but the volume growth of the stand remains unaltered after recovering from the initial thinning shock.

The simulated response of pulpwood production to thinnings during the rotation period was rather small. Heavy thinnings increased pulpwood production, mainly obtained in first thinning (Fig. 8.3a). The response was, however, rather small, only about 20 m^3.

The thinnings increased slightly the simulated log production up to a value of about 300 m^3 (Fig. 8.3b) if the remaining number of trees was more than 40% of the situation before thinning or the removed volume was more than 30% of the stand volume. The 60% reduction in trees by thinning resulted in only a 30% decrease

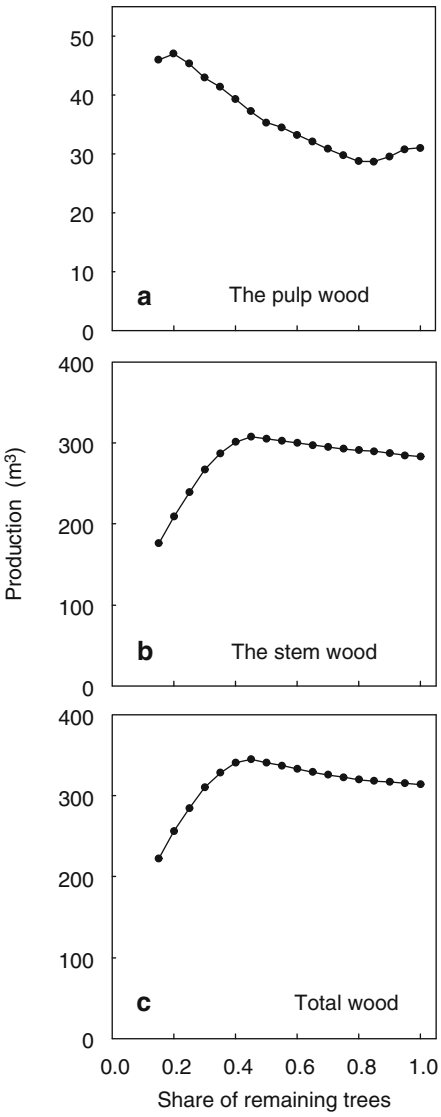

Fig. 8.3 The pulpwood production (**a**), stem wood production (**b**) and total wood production (**c**) during the rotation period as function of the share of remaining trees in the thinnings

in tree volume. Heavier thinnings started to reduce the simulated log production considerably. There is maximum in the total wood production when 40% of the trees remain after thinning (Fig. 8.3c). We have omitted for simplicity the natural mortality in the simulations.

Simulating the stand level responses to management operations has been one of the cornerstones of forest sciences. Determination of optimal rotation periods and timing of intermediate cuttings, not to mention the selection of most appropriate silvicultural methods, require that we are able to estimate properly the forest growth

responses. Various different growth simulators have been developed, and overall, they have served well these purposes (Hyytiäinen et al. 2005). The problem arises in using models that are based on empirical growth function when one needs to extrapolate the growth for conditions that have not been covered in the combinations of conditions used to make these models. There is a possibility for a very unrealistic behaviour, and thus quite often artificial limitations are needed to force the model outcome, and the resulting model behaviour does not necessarily correspond to natural behaviour. This poses problems, particularly if one would want to use mathematical tools to analyse new type of optimal solutions for forest management (Niinimäki et al. 2012). Due to the many degrees of freedom that there are when planning and executing intermediate cuttings over the stand rotations, the problem of extrapolation is easily encountered in connection to stand responses to thinning.

The process-based approach that is based on causal relationships, and that we have used here, has the benefit that the growth of trees is always constrained by the material balances, and grossly unreasonable behaviour is not possible once the specific process rates and stand level interactions are satisfactorily described. The good comparability between simulated and observed stand growth and reasonable behaviour in these initial tests to simulate thinning responses indicate that we are quite close to reaching this situation. The growth behaviour immediately after thinning corresponded to observations of long-term thinning experiments (Eriksson and Karlsson 1997). However, our model predicted faster growth recovery on the long run than was observed. One of the reasons may be that in current simulations, we assumed that nitrogen leaching from the site is negligible. Experiments have shown that removal of logging residue from forests may cause considerable long-term growth reduction (Helmisaari et al. 2011). Similarly, nitrogen leaching from abundant logging residue would produce similar outcome when compared to no leaching assumption.

The many degrees of freedom available when performing thinning make it difficult to describe the responses with traditional methods of forest growth and yield. However, it is also a very challenging task for process-based modelling. As previous chapters have indicated, metabolism, transport and growth are highly integrated phenomena and often produce very tightly confined relationships between process rates and structural quantities, properties and dimensions. These features are widely exploited in the model MicroForest. However, at thinning, growth conditions are abruptly changed; they necessarily trigger a chain of acclimations at different temporal and spatial domains in the remaining trees.

Current results suggest that process-based models, such as MicroForest, are very valuable tools among others for planning optimal forest management. They are capable of simulating that type of information that is required for comparison of different management regimes. The very valuable feature of such models is that the material balances of the forests restrict and constrain the simulations, and therefore completely unrealistic behaviour is impossible in new conditions. This makes dynamic models of forest growth based on carbon and nitrogen balance particularly interesting tools for climate change studies.

8.2.2 The Effect of Whole-Tree Harvesting on the Site Fertility

8.2.2.1 Whole-Tree Harvesting in Forestry

The problem of global warming caused by increasing atmospheric CO_2 concentration stresses the importance finding other energy sources than fossil fuels. Bioenergy, especially the burning of wood and other carbon material obtained from forests has been a leading alternative to fossil fuels. The wood in the stems of trees dominates the biomass in forests, but also the masses of branches and leaves are considerable, and the energy yield can be maximised by whole-tree harvesting. This involves removal of all the above-ground biomass for use in power plants.

Wood has been harvested for centuries from forests, and no evident problems have emerged with the nutrients being removed in the logs. On the other hand, the litter collection from forests to agricultural land has had a negative effect on tree growth, documented centuries ago (see Ebermayer 1876). These facts lead us to the question, does whole-tree harvesting reduce the fertility on the site due to export of nutrients in the leaves and branches?

The model MicroForest is based on the carbon and nitrogen fluxes and pools in a forest ecosystem. Thus, it can be used to analyse the changes, generated by whole-tree harvesting, in the various nitrogen pools and also in stand growth. MicroForest also explains the development of the pools and growth enabling understanding of the changes caused by whole-tree harvesting in a forest ecosystem.

The Finnish Forest Research Institute established experiments 20–30 years ago to study the effects of the whole-tree harvesting on stand growth. The 14 experiments represented a range of site types. The experimental design comprised thinning treatments with or without logging residue removal at establishment. The thinning grade was 16–39% of the standing tree volume. Conventional harvesting of commercially exploitable stem wood with bark served as a control, with logging residues left in the stand and evenly distributed on the plots. In the whole-tree harvesting treatment, the residues were manually removed. At thinning, between 21 and 73 kg N ha^{-1} was removed in logging residues in pine stands and between 58 and 129 kg N ha^{-1} in spruce stands (Helmisaari et al. 2011).

Statistical analysis of the whole-tree harvesting experiments indicated that during the first 10-year period after thinning, the average volume increment was significantly lower on the whole-tree harvesting plots in the spruce stands and tended to be lower ($p = 0.06$) in the pine stands, while in the second 10-year period, the growth decrease was significant also in the pine stands. Volume increment of pine stands was 4 and 8% and that of spruce stands 5 and 13% lower on the whole-tree harvesting plots than on the conventional harvesting plots during the first and the second 10-year periods, respectively. The results confirmed the main hypothesis that whole-tree harvesting decreases tree growth in relation to conventional harvesting, and this change especially depends on the amount of nitrogen removed in logging residues (Helmisaari et al. 2011).

Simulations with MicroForest enables deeper insight into the changes in a forest ecosystem, and this is why we made a complementary analysis of the nitrogen fluxes and pools in stands that are treated with whole-tree harvesting. We think that the nitrogen in the harvested needles and small branches may reduce the pool of reactive nitrogen circulating in the ecosystem, and in this way, whole-tree harvesting may generate growth reduction.

8.2.2.2 Analysis of the Whole-Tree Harvesting with MicroForest

We selected the experimental plot 726 of the Finnish Forest Research Institute for closer study with MicroForest. We used the model developed to describe the stand around SMEAR II measuring station and tested and tuned it using data from additional stands nearby SMEAR II and in Estonia. We utilised the values of the parameters obtained from the measurements at SMEAR II, and we applied the model at the experimental plot number 726 without fitting.

The experiment 726 was established when the stand was 24 years old; before that age, no exact information is available dealing with the stand development. We have the diameters of the trees at the age of 24 years. We ordered the trees according the diameters in the first measurement, and we formed five size classes as in the tests nearby SMEAR II and Estonia, 5% of the biggest trees formed the size class 1, next 15% the class 2, next 30% the class 3, next 30% the class 4 and the remaining 20% the smallest size class 5.

The nitrogen deposition has increased during the later part of the twentieth century, and we assumed that the nitrogen deposition was 0.1 g m^{-2} $year^{-1}$ in the beginning of the simulation and grew linearly to the value 0.4 g m^{-2} $year^{-1}$.

The initial state of the trees in each size class and the protein pool in the soil is needed for the simulations, and this is a bit problematic since about 600 numbers are needed to describe the needle masses, stems and branches and proteins in the soil in MicroForest. We have only the measurements of the stem diameters to determine the initial state. The most practical way to obtain the initial values is to generate them with MicroForest. We varied the initial stem diameters at the age of 4 years and the protein pool in the soil in such a way that simulations with MicroForest resulted into the measured diameters in each size class at the age of 24 years. Then the state of the simulation at the age of 24 years formed all the needed initial values as a coherent set of numbers.

We simulated the stand development during the years 1979–2009 and compared the simulations with the measured stem diameters (Fig. 8.4). The model MicroForest predicted the diameters in each size class rather successfully, and further analysis of the effects of whole-tree harvesting on tree growth with MicroForest seems to be justified.

MicroForest calculates all pools of reactive nitrogen in a forest ecosystem. The amount of reactive nitrogen in the soil determines the fertility of the site since the flux of nitrogen generated by the decomposition of proteins determines the amount of synthesised proteins for the new tissues, especially in the leaves and fine roots.

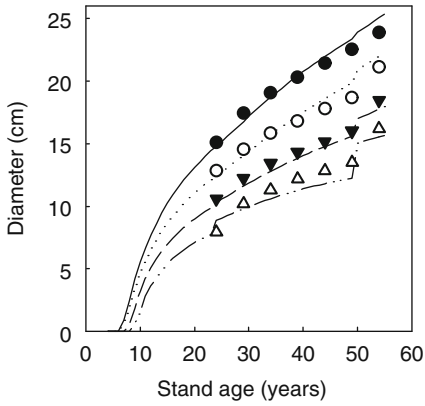

Fig. 8.4 Measured (lines) and predicted (symbols) diameters at the experimental stand 726

The deposition is an additional new source of reactive nitrogen in forest ecosystems. The simulations with MicroForest enable quantification of the reduction in the nitrogen flux from proteins in the soil caused by whole-tree harvesting, and in this way, we obtain also the changes in the growth of the stand.

The proteins in the soil dominate the nitrogen pool in a forest ecosystem; its amount in the simulated initial state at the age of 24 years was 1,300 g m^{-2}. The needle mass changes strongly during the early phase of stand development. When the experiment was established, the simulated needle mass in the stand was stabilising to 400 g m^{-2} containing proteins at about 35 g m^{-2}. The large stem mass in the late phase of stand development makes the protein pool in wood considerable, although the protein concentration is low; this nitrogen is permanently bound into the wood and not circulating in the system. The wood pool was 10 kg m^{-2}, and the protein pool in the wood was 16 g m^{-2} in the beginning of the experiment. The proteins in the bark are missing in MicroForest. The simulated nitrogen flux caused by the decomposition of proteins is 12 g m^{-2} $year^{-1}$ enabling synthesis of 80 g m^{-2} $year^{-1}$ of proteins.

The thinnings at the age of 24 and 49 years of the experiment were rather slight, resulting in about a 35% decrease in the first and 25% in the second thinning in the simulated stand needle mass (Fig. 8.5).

The simulated loss of reactive nitrogen in whole-tree harvesting in the age of 24 years at the experimental plot is 12 g m^{-2}. The observed value of total nitrogen loss was 4.6 g m^{-2} in logging residues and 1.4 g m^{-2} in stem wood. The simulated reduction of the reactive nitrogen in trees and in soil is about 1%.

The simulated effect of whole-tree harvesting on the volume growth was rather small, only about 3% after the first thinning and about 4% after the second one. The comparison with the experimental plots showed a somewhat larger total effect than the empirically measured one. The effect of whole-tree harvesting in this experiment was a 3% reduction in the volume increment during 10–20 years after thinning. During the first 10 years after thinning, there was not yet any effect of whole-tree harvesting.

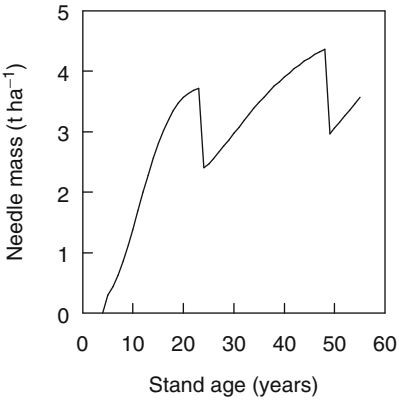

Fig. 8.5 Simulated needle mass in the experimental plot 726

8.2.3 The Effect of Nitrogen Deposition on Forest Production

8.2.3.1 Nitrogen Deposition

The nitrogen circulates between vegetation and soil in a forest ecosystem. The nitrogen deposition, fixation, leaching and evaporation generate small nitrogen fluxes between the ecosystem and its surroundings. The natural flux from the atmosphere to forests has evidently been rather small and stable for millions of years, below 0.1 g m^{-2} $year^{-1}$ (1 kg ha^{-1} $year^{-1}$). The nitrogen fixation is rather weakly known in quantitative terms; however, particularly in northern latitudes, it is also small and of the same magnitude as natural deposition.

The usage of fossil fuels and chemical fertilisers introduced an additional source of reactive nitrogen into the atmosphere. The lifetimes of nitrogen oxides (NO and NO_2) and ammonium in the atmosphere are rather short, only days, and they deposit within some thousands of kilometres from their emission location. Most of the anthropogenic deposition is chemically as ions and readily available for vegetation as a nutrient.

The usage of fossil fuels and chemical fertilisers were rather small before 1950; thereafter, a rapid increase took place, and stabilisation occurred around 1990 in industrialised countries. China and India have dominated the increase in the utilisation of fossil fuels during the last decades. However, increasing traffic continues to be an important and growing nitrogen source also in Europe.

The flux of reactive nitrogen from the atmosphere into forests is rather small when compared with those of water and carbon. There are severe measuring problems involved in the determination of the nitrogen flux from the atmosphere to forests. The wet deposition can be determined from rainwater, but dry deposition is still rather problematic. Small aerosol particles are rich in nitrogen, and they deposit on needles and leaves in forests (Sect. 8.3.6.2) resulting in dry deposition. But that is very problematic to measure. In addition, gaseous nitrogen oxides can deposit directly into leaves (Sect. 4.2.8).

Despite the evident measuring problems, we have rough global picture of the development of nitrogen deposition since 1960 (van Aardenne et al. 2001). The patterns in the development of nitrogen deposition are quite similar in different areas on the globe, a rapid increase, and thereafter, stabilisation reflects the usage of fossil fuels in the industrialised countries. The level of stabile deposition is much higher in the industrialised areas when compared with remote areas far in the north Siberia or Canada. This historical pattern of nitrogen deposition is different in China and India.

The rapid increase in the nitrogen deposition raises the question of the importance of the additional reactive nitrogen in forest ecosystems. The fluxes, and especially nitrogen flux, play an important role in our theory and also in our model MicroForest. Consequently, we use it as a tool to evaluate the role of nitrogen deposition in forests.

8.2.3.2 Simulations of the Effects of Nitrogen Deposition on Forest

We consider in more detail two alternatives: the responses to different increases in nitrogen deposition during the last part of the twentieth century and the response to a step increase in nitrogen deposition.

The patterns of the increase in the nitrogen deposition were similar around the industrialised centres in Europe and America: increase starting around 1950 and stabilisation about 1980 or 1990. We simulate three different deposition patterns:

1. Stable deposition of 0.1 g m^{-2} $year^{-1}$
2. Linear increase from 0.1 to 0.5 g m^{-2} $year^{-1}$ during four decades after 1950 and thereafter stable deposition level
3. Linear increase from 0.1 to 2.0 g m^{-2} $year^{-1}$ during four decades after 1950 and thereafter stable deposition level

The first case refers to the situation before anthropogenic nitrogen deposition, the second one is close to the deposition pattern at SMEAR II station and the third one is possible in Central Europe.

We assumed that the stand was born as even aged in the year 1950 and that the initial state at the age of 4 years was as we measured at Järvselja (Sect. 7.4). We omitted thinnings in our simulations.

The outcome of the simulations is clear. The deposition provides an additional source of nitrogen for the synthesis of proteins, especially in needles and fine roots, and the response is rather large and versatile; the needle mass and stem volume increase (Fig. 8.6). The response saturates at the high deposition and in contrast, the needle mass increases up to the age 80 years in the moderate deposition and the needle mass is rather stable in the case of no anthropogenic deposition. The responses in the stand volume are still larger than in the needle mass.

The responses in needle mass and in photosynthesis are fairly small when compared with the stem volume. The nitrogen deposition generates large changes in allocation, and this change is the key to understand the obtained simulation. The fine

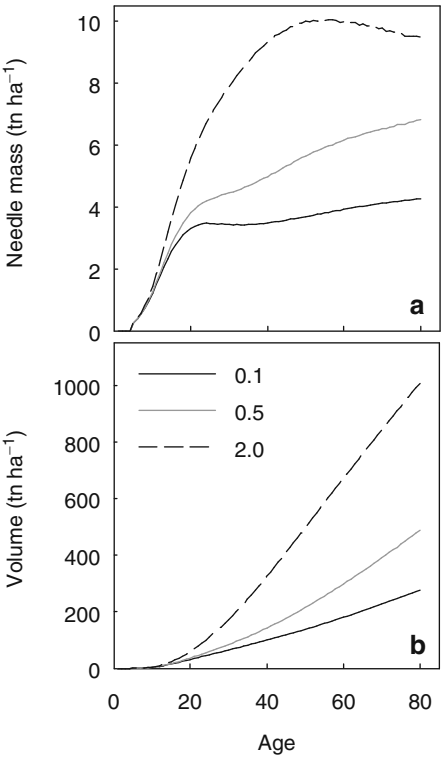

Fig. 8.6 The simulated needle mass (**a**) and stand volume (**b**) as function of stand age at varying nitrogen deposition. We simulated three deposition patterns: (i) stable deposition 0.1 g m^{-2} year^{-1}, (ii) linear increase from 0.1 to 0.5 g m^{-2} year^{-1} during four decades and there after stable 0.5 g m^{-2} year^{-1} and (iii) linear increase from 0.1 to 2.0 g m^{-2} year^{-1} during four decades and there after stable 2.0 g m^{-2} year^{-1}

roots and mycorrhiza are the biggest single sink of sugars formed in photosynthesis if the nitrogen deposition is 0.1 g m^{-2} year^{-1}, and if the nitrogen deposition is as high as 2 g m^{-2} year^{-1}, then the share of roots and mycorrhiza is negligible. This simulation result comes from the fundamental logic of MicroForest. When the deposition increases the availability of nitrogen, the solution of the nitrogen and carbon balance equations results in smaller allocation to roots and mycorrhiza, and the remaining sugars can be used for stem and needle growth.

Our simulations omit the increase in leaching due to the nitrification and gaseous nitrogen losses due to denitrification. Thus, our simulations may result too high response at high deposition.

The simulations that mimic the observed and expected nitrogen deposition indicated that the forests can response with increasing growth to stable deposition for decades. This raises the question, how long are the forests able to accelerate their growth under stable anthropogenic nitrogen deposition?

We simulated the response of forests' ecosystem to step increase in deposition to find the time constant of the response. We assumed stable low nitrogen deposition, that is, 0.1 g m^{-2} year^{-1} for the first 30 years of the ecosystem development, and after the year 30, the deposition was constant either 0.5 or 2 g m^{-2} year^{-1}. For comparison, we simulated also the case of stable nitrogen deposition (Fig. 8.7).

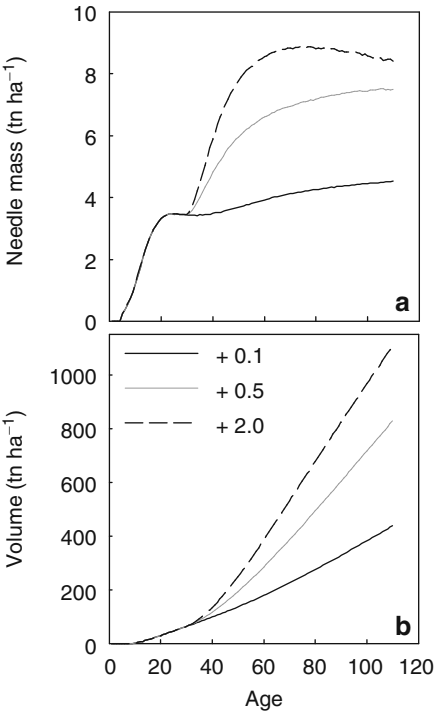

Fig. 8.7 The simulated needle mass (**a**) and stand volume (**b**) as function of stand age at different levels of step increase in nitrogen deposition at the age of 30 years. We applied three increases: (i) from 0.1 to 2.0 g m^{-2}, (ii) from 0.1 to 0.5 g m^{-2} and (iii) stable 0.1 g m^{-2} for comparison

The reactive nitrogen accumulated nearly 50 years into the ecosystem at low anthropogenic deposition, and the release of nitrogen from proteins in soil indicates stabilisation 50 years after the beginning of the additional nitrogen deposition. The stabilisation of the proteins in the soil is reflected also to other components in the system.

At high deposition, the response saturated clearly faster than at low level. On average, the time constant of the response to sudden increase in the nitrogen deposition is roughly about 50 years, at low deposition longer and at high shorter than that. The increased anthropogenic nitrogen deposition stabilised to the present high level some decades ago. Thus, forest ecosystems are still accumulating reactive nitrogen, and the responses are increasing. Deposition provides additional reactive nitrogen that accumulates into forest ecosystems in needles and especially into proteins in the soil. The extra nitrogen enables construction of additional needles, and in this way, the photosynthesis of the ecosystem increases providing additional sugars for growth of wood in stems and branches. Although the nitrogen deposition is small, usually less than 2 g m^{-2} year^{-1}, its accumulation into forest ecosystems generates large effects.

We omit in our simulations the changes in leaching and gaseous release from the forest soil. The concentrations of ammonium and nitrate ions in soil solution will increase due to the nitrogen deposition, and the seepage water will carry nitrogen

into ground water. In addition, the nitrification (Sect. 4.4) and denitrification will generate outflow of N_2 and N_2O. The omitting of leaching and gaseous outflow of nitrogen generates bias in our simulations, and the obtained values are evidently too large. However, the deposition levels as observed at SMEAR II have not yet caused any measurable loss of accumulated nitrogen, and in this respect, the result can be considered more realistic. Indeed, the growth of Finnish forest has doubled from 1950s. Much of this change can be contributed to silviculture and changing age structure, but certainly, there has also been fertilisation effect from nitrogen deposition as well.

8.3 Climate Change and Forests

8.3.1 Physical Background of Climate Change

Timo Vesala, Jouni Räisänen, Tuukka Petäjä, Erkki Siivola, and Pertti Hari

The solar radiation energy (1.37 kW m^{-2} through a tangential plane above the atmosphere, Sect. 3.2) generates processes and transport of entities on the planetary surface and in the atmosphere. The processes, principally the absorption and emission of radiation, evaporation, condensation, freezing and melting of water, convert the energy into different forms giving rise to concentration, temperature and density differences that generate material and energy flows within the atmosphere and between the atmosphere and the surface of the globe. These processes and material and energy flows determine the climate on the globe. The conservation of mass, energy and momentum plays a key role in the combining of different phenomena. The behaviour of the atmosphere can be concisely expressed in seven differential equations. The increasing concentrations of greenhouse gases reduce the thermal radiation of the globe into the space generating climate change. The global climate models, based on the seven atmospheric equations, are able to produce the present climate and also the increasing trend in temperature.

Our approach, when we analysed the behaviour of trees, forest soil and forest ecosystem in Chap. 5, was based on the processes generating concentration, temperature and pressure differences that give rise to material and energy flows within trees and ecosystem and between ecosystem and its environment. The conservation of mass and energy plays an important role in the combination of different phenomena. Evidently, our approach in Chap. 5 is very similar to that applied in the meteorology when the behaviour of the atmosphere is analysed.

T. Vesala (✉)
Department of Physics, University of Helsinki, P.O. Box 48,
00014 University of Helsinki, Helsinki, Finland
e-mail: timo.vesala@helsinki.fi

Several processes convert solar energy in the atmosphere into other forms. Absorption in the atmosphere and on the Earth's surface transforms this radiation energy into heat warming the atmosphere. Emission of thermal radiation and transpiration and evaporation processes cool and condensation of water vapour releases heat. Heat exchange tends to level temperature differences. Pressure and temperature differences generate vertical and horizontal flows in the atmosphere. Conservation of mass, energy and momentum forms the basis for the quantitative analysis of the behaviour of the atmosphere (see Basic idea 9, Chap. 2).

8.3.1.1 Phase Transitions

First-order phase transitions, like freezing-melting and condensation-evaporation of water, are associated with heat of transition. The phase transitions are important for the behaviour of the atmosphere since they release and absorb energy affecting distribution and transport of it. *Evaporation* needs external energy which is transported from surroundings, and the surface temperature with evaporating water tends to be lower than the ambient one. Correspondingly, in *condensation*, heat is released and transported to surroundings, and the surface temperature is elevated. When phase transitions occur, they must be taken into account in any considerations of energy balances and exchange. Transpiration is physical evaporation from wetted interfaces along the pores in the cell walls of mesophyll, epidermal and guard cells, via stomatal openings to the atmosphere, lowering the leaf temperature. Conversely, a leaf can gain latent heat if dew or frost condenses onto it (see Nobel 2005). Note that evaporation and condensation are reverse processes, and the amount of heat required to vaporise liquid water is the same as the released heat if the same amount of water vapour is condensed to liquid. The latent heat of vaporisation of water is 2,260 kJ kg^{-1} and the same amount is released in condensation.

Freezing and melting are other relevant examples of phase transitions, and, similarly to evaporation/condensation, external energy is needed for melting and the same amount is released in freezing. The latent heat of freezing of water is much smaller than the heat of vaporisation, only 333 kJ kg^{-1}.

8.3.1.2 Electromagnetic Radiation

The atmosphere and surfaces of solid objects absorb and emit electromagnetic radiation. Conservation of energy means that absorption and emission are always connected with temperature changes, which has strong consequences to the behaviour of the atmosphere. All materials emit radiation since there is a tendency for the atoms and molecules to return spontaneously to lower energy states (see Bird et al. 2002), and in this process energy is emitted. Because the emitted radiation results from changes in the electronic, vibrational and rotational states of the atoms and molecules, the radiation is distributed over a range of wavelengths.

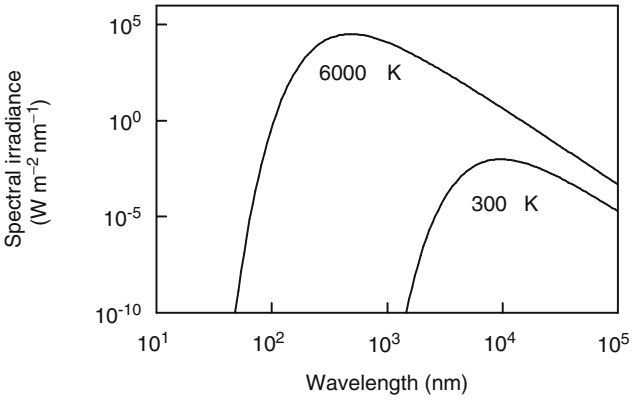

Fig. 8.8 Black-body spectra for 6,000 and 300 K. The temperatures correspond to surface temperature of the Sun and the Earth, respectively. The spectrum of black body at 300 K is invisible in the linear scale

Let us consider first a so-called *black body*, a perfectly efficient emitter, which has a surface emitting hemispherically isotropic radiation at all frequencies. Many natural objects are an approximation to this idealised body. Irradiance $I_{E,\lambda}$ as a function of wavelength (λ) and surface temperature (T) can be approximated with Planck's law of black-body radiation (e.g. Bird et al. 2002):

$$I_{E,\lambda}(\lambda,\ T) = \frac{2\ \pi\ h\ c^2}{\lambda^5} \cdot \frac{1}{e^{c\ h/k\ \lambda\ T} - 1}, \tag{8.1}$$

where c, h and k are speed of light in vacuum (2.9979×10^8 m s^{-1}), Planck's constant (6.626×10^{-34} J s) and Boltzmann's constant (1.381×10^{-23} J mol^{-1} K^{-1}), respectively. Planck's law is one of the triumphs of explaining observed phenomena by using quantum mechanics. It can be derived by applying quantum statistics to a photon gas (or generally to a system of elementary particles called bosons) in a cavity, the photons obeying Bose-Einstein statistics (Bird et al. 2002).

Theoretical spectral irradiance of two black bodies of 6,000 and 300 K are depicted in Fig. 8.8. The selected temperatures are close to the surface temperatures of the Sun and the Earth or any bodies on Earth. The Planck distribution predicts the entire energy versus wavelength curve and the shift of the maximum towards shorter wavelengths at higher temperatures. In fact, the emission spectrum of many bodies at room temperature is very close to 300-K black-body spectrum in Fig. 8.8, and the spectrum of Sun radiation (detected outside the atmosphere) is very close to 6,000-K black-body spectrum (Figs. 8.8 and 8.9) The solar spectrum has a maximum in visible light wavelengths, whereas terrestrial radiation emitted into space has a maximum approximately at 10 μm (infrared).

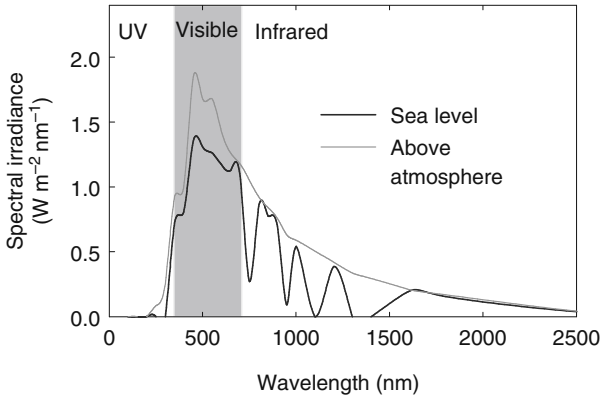

Fig. 8.9 A simplified wavelength distribution of radiative energy from the Sun outside the Earth's atmosphere and at sea level

For non-black surfaces, the emitted energy flux is

$$I_E = e\ \sigma\ T^4, \tag{8.2}$$

where e is the *emissivity* and must be evaluated at temperature T. Unoxidised, clean, metallic surfaces have very low emissivities (like 0.02 for polished copper), whereas most nonmetals and metallic oxides have emissivities above 0.8 at room temperature, and natural/biological surfaces have e of nearly 1.0. The emissivity increases with increasing temperature for nearly all materials. Note that the emissivity may depend on the frequency of radiation. If it is <1 but is the same over all frequencies, the body is called grey.

Formula 8.2 has been effectively used in measurements of surface temperatures of bodies, by infrared sensors and cameras. If the surface emissivity is known, the measured energy flux can be readily inverted to the temperature by the formula.

8.3.1.3 Interaction of Radiation and Matter

The functioning of all land ecosystems is driven by radiative energy from the Sun. Light energy directly drives photosynthesis and transpiration in plants and also affects stomatal action and the rates of biological processes, such as respiration, through temperature by warming up the plants. Infrared energy, which is about half of all the incident energy from the Sun, has a significant warming effect and thus increases the tendency of water to be evaporated from leaves in transpiration.

Photons interacting with material are either absorbed, reflected or transmitted through the material. The fraction of incident radiation flux density that is absorbed

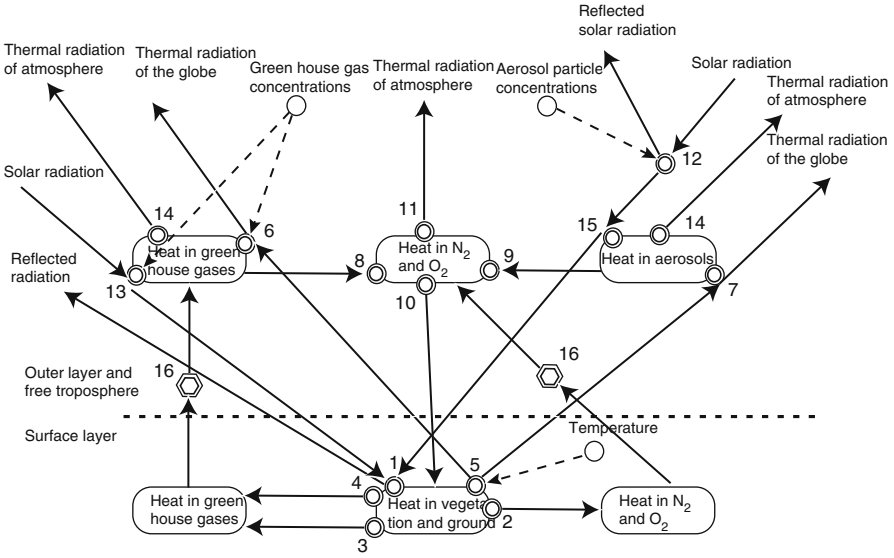

Fig. 8.10 Energy exchange, transport and storages in the atmosphere-biosphere continuum daytime. The atmosphere can be divided into several layers, but here only the surface layer is indicated since ecosystems are located there. The surface layer is located within the atmospheric boundary layer and the boundary layer above the surface layer is called the outer layer (see, e.g. Arya 2001). The free troposphere extends above the boundary layer up to the tropopause. Heat in N_2 and O_2 includes also a contribution from non-greenhouse gases. Note that aerosols include also clouds since physically cloud is aerosol. The *circles* represent environmental factors, *hexagons* physical properties, *double hexagons* transport, and *double circles* processes, *arrows* material/energy flow and *dashed arrows* influence (Fig. 2.3)

by a surface is called absorptivity. Reflectivity is the fraction that is reflected by a surface, and transmissivity is the fraction that is transmitted through a surface. The sum of absorptivity, reflectivity and transmissivity equals 1.

Scattering is a physical process where radiation is forced to deviate from a straight trajectory by the particles in the medium through which the radiation passes. In solid or liquid medium, scattering results in part of the incident radiation being reflected from the surface. Also photons absorbed by the medium or transmitted through it may have undergone scattering in the medium. Because scattering depends on wavelength, the spectral composition of scattered (diffuse) light is altered from that in the Sun's direct beam. The spectrum of diffuse light in a clear sky is shifted towards shorter wavelengths and thus appears blue to the human eye. Under clouds, scattering causes the sky to be greyish. Correspondingly, the spectrum of light inside a tree canopy is different from the spectrum of incoming solar radiation: light transmitted through or reflected from foliage is enriched in green because blue and red wavelengths are absorbed by photosynthetic pigments in the leaves.

8.3.1.4 Heat Transport and Exchange in the Atmosphere and Between Atmosphere and Surface

Here, we discuss on a general level the conservation and transport of energy in the atmosphere. Energy input by solar radiation is the 'engine' driving the processes and the associated transport phenomena in the atmosphere and biosphere. The numbers in the following discussion refer to Fig. 8.10. A fraction of the energy carried by solar radiation penetrates the atmosphere and is absorbed at the surface (1). The heated surface warms the adjacent air layers composed of nitrogen, oxygen and, to a lesser extent, greenhouse gases (GHG) including water vapour (2 and 3). Conduction and convective transport are coupled with evapotranspiration (4), which transforms a fraction of heat from the absorbed radiation to the latent heat associated with vaporised water vapour. The surface emits thermal (long wave) radiation (5). A part of the incident solar radiation is reflected, this fraction being termed the surface albedo. A large fraction of the thermal radiation is absorbed by greenhouse gases (6), clouds (7) (in Fig. 8.10 aerosols include also clouds). Absorbed energy is distributed to the main materials of the air (8 and 9), nitrogen and oxygen and further transported by thermal radiation (10 and 11) and convection. Not all solar radiation penetrates to the surface; some is reflected (12) mainly by clouds and absorbed (13) mainly by gases such as water vapour and ozone and by aerosols (15). The absorbed energy is redistributed among gases and radiated away (14). Convection, that is, bulk flow, transports heat and latent energy vertically and horizontally in the atmosphere. The overall energy balance is maintained by the outward thermal radiation of the atmosphere (11 and 14). This is the key issue in understanding the greenhouse effect. The atmosphere containing the increased concentration of GHGs is more opaque for thermal radiation, and thus the loss of heat by outward thermal radiation occurs effectively from upper atmospheric layers. Upper layers are however colder, and thus the intensity of radiation tends to be reduced. For maintaining the (radiative) energy balance, the temperature is consequently increased at the lower atmosphere.

Figure 8.10 represents the daytime situation when insolation is at high levels. At night and occasionally also on winter days at high latitudes, the solar radiation component is naturally missing or is very low, and thermal radiation (4) may effectively cool the ground surface and surface layer.

8.3.1.5 Conservation Principles

The conservation principles of mass, energy and momentum are fundamental theoretical principles in classical physics as well as in quantum mechanics and the theory of relativity. For phenomena considered in this book, the theory of relativity and quantum mechanics *per se* can be ignored, although they are needed, for example, in fundamental understanding of electromagnetic radiation. The conservation principles in classical physics have been tested since the Newtonian era, and they have passed the tests very successfully. In fact, modern technology can be seen in general as rigorous tests of conservation principles.

The conservation of basic entities sets a strict framework for analysis, which any solution of a problem and a model must follow. An excellent and thorough discussion on conservation principles in the context of transport phenomena is given by Bird et al. (2002). In derivations of conservation equations, one considers the volume element where the amounts of momentum, heat and mass may change, and those changes are balanced by transport of the quantities through the volume boundaries and the rate of production within the volume. The equations are thus derived from a fundamental concept of conservation where the phenomenological transport mechanisms are embedded, and the fluxes are replaced by expressions involving transport properties and gradients of concentration, velocity and temperature. This enables the derivation of formulas that form a closed set of equations for velocity components, temperature, concentration, pressure and density (see Chap. 2, Eq. 2.3).

8.3.1.6 Basic Equations of Atmospheric Models

General circulation models (GCM) are invaluable tools in analysis of past, present and future climate and are thus linked with many themes presented in this book. There is a debate on how much we can trust complicated numerical models. However, it is demonstrated below that in fact the basic formulas are very simple, and they are rigorously based only on conservation principles and transport equations and do not contain any esoteric components. The analysis of atmospheric flows normally utilises some coordinate transforms, but they are just straightforward mathematical treatments.

Present GCMs are based on so-called *hydrostatic primitive equation*s, which are normally formulated in Cartesian *pressure coordinates*. At synoptic scale (∼1,000 km), the atmospheric flows are very close to incompressible flows, and the condition of hydrostatic balance provides an excellent approximation for the vertical dependence of the pressure field in the real atmosphere (Holton 2004).

The seven differential equations in the Box 8.1 form a full set with as many equations as there are unknowns and in principle they describe the behaviour of the atmosphere very accurately. The atmosphere is divided into grid boxes, and conservation laws are applied for each box. However, as computing resources make it necessary to use a rather coarse grid, small-scale processes, like turbulence and convective clouds, cannot be solved directly. Even their numerical treatment is difficult. The challenge is to calculate ‘the source terms’ of turbulent friction, diabatic heating and phase transitions accurately enough since they describe the processes occurring in spatial scales smaller than the typical grid size of the numerical model. However, the source terms are very important in simulations of climate and its changes.

Box 8.1

The atmospheric equations in the rotating pressure coordinates are as follows:

Equation for west–east wind u:

$$\frac{\partial u}{\partial t} = -u\frac{\partial u}{\partial x} - v\frac{\partial u}{\partial y} - \omega\frac{\partial u}{\partial p} - \frac{\partial \Phi}{\partial x} + fv + F_x \tag{8.3}$$

Equation for south–north wind v:

$$\frac{\partial v}{\partial t} = -u\frac{\partial v}{\partial x} - v\frac{\partial v}{\partial y} - \omega\frac{\partial v}{\partial p} - \frac{\partial \Phi}{\partial y} - fu + F_y \tag{8.4}$$

Thermodynamic equation (energy conservation):

$$\frac{\partial T}{\partial t} = -u\frac{\partial T}{\partial x} - v\frac{\partial T}{\partial y} - \omega\frac{\partial T}{\partial p} + \omega\frac{RT}{C_p p} + \frac{Q}{C_p} \tag{8.5}$$

Hydrostatic balance equation:

$$\frac{\partial \Phi}{\partial \mathrm{p}} = -\frac{RT}{p} \tag{8.6}$$

Equation of continuity (mass conservation):

$$\frac{\partial u}{\partial x} + \frac{\partial v}{\partial y} + \frac{\partial \omega}{\partial p} = 0 \tag{8.7}$$

Continuity equation (water vapour concentration q):

$$\frac{\partial C_{\mathrm{H_2O}}}{\partial t} = -u\frac{\partial C_{\mathrm{H_2O}}}{\partial x} - v\frac{\partial C_{\mathrm{H_2O}}}{\partial y} - \omega\frac{\partial C_{\mathrm{H_2O}}}{\partial p} + S_{\mathrm{H_2O}} \tag{8.8}$$

Continuity equations for other species A:

$$\frac{\partial C_{\mathrm{A}}}{\partial t} = -u\frac{\partial C_{\mathrm{A}}}{\partial x} - v\frac{\partial C_{\mathrm{A}}}{\partial y} - \omega\frac{\partial C_{\mathrm{A}}}{\partial p} + S_{\mathrm{A}} \tag{8.9}$$

where $\omega = (\mathrm{d}p/\mathrm{d}t)$ is usually called the 'omega' vertical motion, the pressure change following the motion. It plays the role of the vertical wind in the pressure coordinate system. Φ is the geopotential equal to gz where g is the gravity including also the apparent centrifugal acceleration due to rotation of the Earth. The geopotential at the height of z is the work required to raise a unit mass to height z from mean sea level that is the potential energy per unit mass. f is the Coriolis parameter equal to $2\Omega \sin \phi$ where Ω is Earth's angular speed of rotation and ϕ is latitude. F_x and F_y describe the turbulent friction in the atmospheric boundary layer (ABL). R is the gas constant of air. Q involves the diabatic heating, including most importantly radiation and phase transitions of water. $S_{\mathrm{H_2O}}$ describes effects of evaporation and condensation to water vapour concentration.

8.3.2 *Mechanisms of Climate Change*

Jouni Räisänen and Heikki Tuomenvirta

The increasing concentrations of CO_2 and other greenhouse gases change the behaviour of radiation energy in the atmosphere. Several processes (Sect. 8.3.1) respond to this redistribution of radiation. The above conservation equations of mass, energy and momentum can be solved numerically to study the resulting effects on climate.

Changes in climate occur both as a result of natural variability and as a response to anthropogenic forcing. Some part of the natural variability is forced, that is, caused by external factors such as solar variability and volcanic eruptions. Another part is unforced, associated with the nonlinear internal dynamics of the climate system such as interactions between the atmosphere and the oceans. Because of these natural mechanisms, climate has always varied, on time scales ranging from years to millions of years (Jansen et al. 2007), and it would continue to vary in the future regardless of what mankind is doing. Nevertheless, when we focus on this and the following centuries, the effects of natural variability will likely be secondary when compared with anthropogenic changes in the global climate (Meehl et al. 2007).

Anthropogenic climate change is often referred to simply as *global warming* (e.g. Harvey 2000; Houghton 2004). This refers to the expected tendency of increased greenhouse gas concentrations to warm up the surface and the lower atmosphere in all or nearly all parts of the world. Nevertheless, other anthropogenic forcing mechanisms such as changes in land use and, in particular, increased aerosol concentrations complicate this picture (Forster et al. 2007). Furthermore, although temperature is the climate variable in which the anthropogenic changes are expected to be strongest when compared with natural variability, many other aspects of climate will also change.

The Earth has a *natural greenhouse effect* which helps to keep the surface of our planet much warmer than it would otherwise be. The surface of the Earth emits thermal radiation almost like a black body, with the intensity of radiation increasing with the fourth power of the surface temperature (Jin and Liang 2006; Eq. 8.2). On the other hand, considering the energy budget of the Earth and its atmosphere as a whole, there must be a close balance between the solar radiation absorbed by our planet and the thermal radiation escaping to space. From this condition, it follows that if the atmosphere were transparent to thermal radiation, the average surface temperature of the Earth would be only about −18°C (255 K). The observed mean surface temperature is about 32°C higher. This difference is due

J. Räisänen (✉)
Department of Physics, University of Helsinki, P.O. Box 48,
00014 University of Helsinki, Helsinki, Finland
e-mail: jouni.raisanen@helsinki.fi

to the fact that most of the thermal radiation emitted by the surface is absorbed by the atmosphere, and the radiation that actually escapes to space therefore has its origin in atmospheric layers much cooler than the surface. Of the so-called *greenhouse gases* that are responsible for this effect, the most important is water vapour (with a contribution of about 60% in clear-sky conditions), followed by carbon dioxide CO_2 (26%) and ozone O_3 (8%). Methane (CH_4) and nitrous oxide (N_2O) together account for the remaining 6% (Kiehl and Trenberth 1997). Clouds also amplify the greenhouse effect, with a contribution comparable to that of CO_2, but this is more than compensated by their ability to reflect solar radiation to space.

We have very little information about conditions on the globe in the distant geological past. However, some materials can be found which can be dated and which reflect air temperature or gas concentrations characteristic of their formation period. The most valuable sources of information for the most recent 800,000 years are ice cores taken from the Antarctica or Greenland. Small air bubbles in the ice enable the determination of atmospheric CO_2 concentrations when the ice was formed from accumulating snow. In addition, the ratio of stable oxygen isotopes reflects the temperature conditions of the ocean around the Arctic and Antarctic regions.

Ice cores that have been extracted from Antarctica and Greenland indicate that the atmospheric CO_2 concentration has varied in a range from 180 to 300 ppm during the last 800,000 years (Fig. 8.11a). The stable isotopes of oxygen indicate that temperature has varied simultaneously with the atmospheric CO_2 concentration. Periods of low atmospheric carbon dioxide concentration (glacials) have been cooler than those of high concentration (interglacials, including the last 10,000 years) (Fig. 8.11b). This is thought to reflect a positive feedback between carbon cycle and climate. Variations in carbon dioxide concentration have been ultimately driven by changes in climate, but they have also acted to amplify the glacial-interglacial temperature variability.

Changes in atmospheric carbon dioxide concentration during the glacial-interglacial cycles have been slow; they have happened on a time scale of 10,000 years. This tells us that the natural carbon cycle has been closely balanced. Each year, vegetation assimilates about 15% of all the carbon dioxide in the atmosphere by photosynthesis, but nearly the same amount of carbon dioxide is returned to the atmosphere by respiration and decomposition. Similarly, although large amounts of carbon dioxide are dissolved in oceans, especially the northern oceans, this is compensated by outgassing of carbon dioxide back to the atmosphere in other ocean areas. During the past 10,000 years preceding the industrial era, this balance was even more perfect, and the atmospheric CO_2 concentration was stable at about 260–280 ppm. During the same period, temperatures were also relatively stable and warmer than average according to the ice core data.

The slow natural changes in carbon dioxide concentration as seen in the ice core record contrast strongly with the rapid increase during the industrial era and particularly the last few decades (Fig. 8.11a). The concentrations of methane CH_4 and N_2O in the atmosphere have also had a strong increasing trend during the same period.

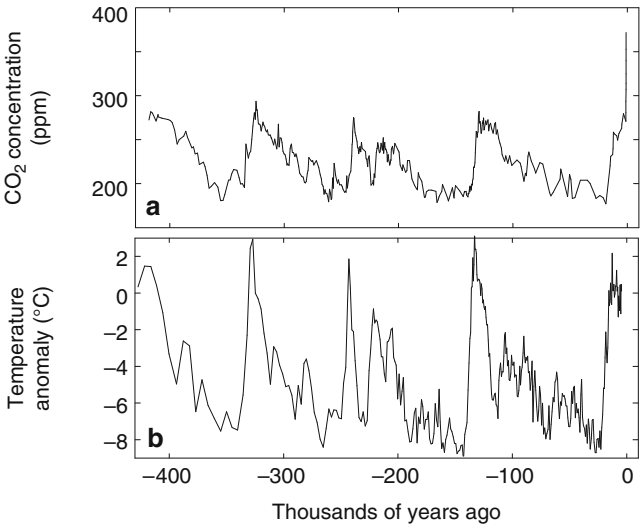

Fig. 8.11 Concentration of CO_2 (**a**) and development of temperature (**b**) during the last 420,000 years. The concentration data are compiled from three sources, (i) Vostock ice cores (Barnola et al. 2003), (ii) Siple station ice core data (Friedli et al. 1986) and (iii) atmospheric measurements (Keeling and Worf 2005). The temperatures are determined from Vostok ice core isotopes as difference from present values (Jouzel et al. 1987, 1993, 1996; Petit 1999)

The absorption of radiation energy by gases depends strongly on the wavelength, the radiation can penetrate a gas without absorption at some and it can be totally absorbed at some other wavelength. The absorption by the atmosphere depends strongly on the wavelength; at visible light (380–740 nm), the absorption is very small, and at some wavelengths in the infrared (740 nm to 300 μm) area, the atmosphere is opaque (Fig. 8.9). The increasing concentrations of CO_2, CH_4 and N_2O enhance the absorption at wavelengths at which the atmosphere is at least partially transparent, and the greenhouse gases can absorb radiation.

Because of human activities, the concentrations of many greenhouse gases have increased and are projected to increase further in the future. The effect that a given change in the atmospheric composition has on the planetary energy budget is commonly quantified by *radiative forcing*. This measures, in approximate terms, the change in the energy balance of the Earth-atmosphere system that a given change in external conditions would induce with no compensating changes in climate (for the exact definition, see Houghton et al. 2001, p. 795). For the increase in CO_2 concentration from pre-industrial time to the year 2005 (280–379 ppm), the radiative forcing was approximately 1.66 W m^{-2} (Forster et al. 2007), and it is currently increasing by about 0.03 W m^{-2} $year^{-1}$. Smaller positive forcing contributions have come from increases in CH_4 (0.48 W m^{-2}), N_2O (0.16 W m^{-2}), various halocarbons (0.34 W m^{-2}) and tropospheric O_3 (0.35 W m^{-2}). With the

exception of O_3, all these forcings can be estimated with a good accuracy ($\pm 10\%$) because the radiative properties of gas molecules are well known, and the lifetime of these greenhouse gases (excluding O_3) is long enough to make them almost evenly distributed in the lower atmosphere. All in all, the present-day radiative forcing from anthropogenic increases in greenhouse gas concentrations approaches 3 W m^{-2}. This number does not include changes in water vapour because direct anthropogenic sources of water vapour are negligible when compared with the natural hydrological cycle. However, observations suggest that water vapour is increasing in response to observed atmospheric warming and is thereby providing a positive feedback to ongoing climate change (Trenberth et al. 2007).

Greenhouse gas forcing has, however, been partly compensated by a net negative forcing from increased aerosol loading. The direct effect of anthropogenic aerosols, associated with the scattering and absorption of solar radiation by aerosol particles, varies in sign between different aerosol types, but the net forcing is very likely negative. In its 4th Assessment Report (Forster et al. 2007), the Intergovernmental Panel on Climate Change gives it a best estimate of -0.5 W m^{-2} and a wide estimated uncertainty range of -0.1 to -0.9 W m^{-2}. The anthropogenic increase in aerosols also results in an increase in available cloud condensation nuclei, which has the potential to increase cloud albedo. The negative forcing due to this indirect aerosol effect is estimated as -0.7 W m^{-2}, but with a very wide uncertainty range (-0.3 to -1.8 W m^{-2}). Furthermore, aerosols may also affect the lifetime of clouds and hence the total cloud cover, but this effect is even more poorly quantified.

As the anthropogenic increase in aerosol loading has resulted in a negative radiative forcing, it has most likely slowed down the warming that would have resulted from increases in greenhouse gas concentrations alone. However, the magnitude of the aerosol forcing and hence the degree of this compensation is poorly known (e.g. Andreae et al. 2005). Also in contrast to the more or less evenly distributed greenhouse gas forcing, the aerosol forcing is concentrated in the vicinity of areas with the largest aerosol-generating emissions (e.g. Forster et al. 2007). Thus, greenhouse gas-induced and aerosol-induced climate changes are expected to have partly different geographical distributions. However, these differences are moderated by atmospheric circulation, which tends to spread the effects of even localised forcings to the global scale (e.g. Boer and Yu 2003).

Positive radiative forcing tends to increase, and negative forcing decrease the global mean temperature, but the magnitude of the forcing does not directly tell the magnitude of the temperature response. The latter depends on several feedbacks acting in the climate system, and it therefore needs to be estimated with climate models. However, model simulations suggest that the ratio of the response to the magnitude of forcing is approximately the same for different forcing agents (e.g. Joshi et al. 2003; Hansen et al. 2005).

In the absence of amplifying feedbacks, the global climate would be quite resistant to radiative forcing. For example, a hypothetical doubling of the atmospheric CO_2 concentration, which gives a radiative forcing of about 3.7 W m^{-2}, would result in a global mean warming of only about 1.2°C, once the climate has had sufficient

time[1] to reach a new equilibrium (e.g. Hansen et al. 1984). In fact, this number, known as *climate sensitivity,* is most likely higher, but its exact value is very hard to determine. According to the latest estimates, which combine evidence from model simulations and observations (Meehl et al. 2007), it is probably within the range 2–4.5°C.

The water vapour holding capacity of air increases quasi-exponentially with increasing temperature by approximately 7% for each 1°C of warming. Assuming that there will be no large changes in relative humidity, which is supported by both observations and model simulations (Held and Soden 2006), the actual concentration of water vapour will also increase. Because water vapour is the most important greenhouse gas in the atmosphere, the increase in its concentration will result in a strong positive feedback. Another most likely positive feedback is associated with changes in snow and ice cover. With a warming of climate, ice and snow cover will be most likely reduced, which increases the solar radiation absorbed at the surface and therefore acts to amplify the warming. This feedback is particularly important in high latitudes, but its role in amplifying the global mean warming is expected to be smaller than the role of increasing water vapour (Webb et al. 2006).

Clouds are important for the global climate, as they both reflect solar radiation to space (a cooling effect) and absorb thermal radiation emitted by the surface (a warming effect). Changes in cloudiness may thus also result in an important feedback effect. However, the complexity of cloud dynamics and microphysical processes makes this feedback very difficult to determine, although the most recent model estimates suggest that it will also probably be positive (Colman 2003; Webb et al. 2006). As a result, changes in cloudiness appear to be the most important uncertainty in the response of climate to increasing greenhouse gas concentrations (e.g. Webb et al. 2006).

The interaction between biosphere and climate may also result in feedbacks. Focusing, in particular, on the role of boreal forests, there are several possible feedbacks:

1. The model simulations discussed in Sect. 8.3.5 suggest that the growth of boreal forests will increase with increasing temperature. This will cause the trees to sequester more CO_2 from the atmosphere, which represents a negative feedback to the climate system. On the other hand, decomposition of organic matter in the soil is also expected to accelerate with warming. The net effect of boreal forests on the CO_2 concentration will depend on which of these competing feedbacks dominates (Friedlingstein et al. 2006).
2. Model simulations also point to an increase in the leaf area index of the trees in a warmer climate, which has the potential to increase transpiration. This may have multiple effects on climate. Increased transpiration is expected to increase water vapour concentration in the atmosphere, thus amplifying the greenhouse

[1] Due to the large heat capacity of the oceans, this equilibration time is of the order of centuries.

effect. On the other hand, the resulting increase in humidity is also expected to promote formation of low clouds, which will reduce the solar radiation reaching the surface. Finally, an increase in transpiration would leave a smaller fraction of the available radiation energy for heating the surface that, like increases in cloudiness, would tend to reduce the surface temperature.

3. Increased activity of the forest canopy can also lead to an increase in the formation of biogenic aerosols, with implications on the scattering of solar radiation and cloud formation.
4. Increases in the leaf area index and the density of the forest canopy may reduce the surface albedo, particularly during the snow season when the albedo contrast between mostly snow-free tree crowns and open snow-covered land is large. This positive feedback is potentially important, particularly during late winter and early spring when there is still snow on the ground, but a lot of solar radiation is already available. Simulations with coupled climate-vegetation models suggest that this feedback may have played an important role in explaining the relative warmth of the northern hemisphere high-latitude continents during the mid-Holocene 6,000 years ago (e.g. Wohlfahrt et al. 2004).

8.3.3 Observed and Projected Changes in Climate

Jouni Räisänen and Heikki Tuomenvirta

The longest series of direct meteorological observations in the boreal region cover over 200 years. For example, in Stockholm (Moberg et al. 2002) and St. Petersburg (Jones and Lister 2002), air temperature and pressure have been measured since the mid-eighteenth century. However, only from the latter part of the nineteenth century have there been enough stations to calculate the global and boreal zone area-averaged temperatures. For the other parameters describing climatic conditions, such as precipitation amount, data coverage and its accuracy are limited until the twentieth century. Increasingly comprehensive observations are only available, for example, for snow cover and water vapour, during the recent decades. In this section, we will describe succinctly what kind of changes have been observed in the boreal climate.

The global mean temperature has increased 0.8 ± 0.2°C since the late nineteenth century (Trenberth et al. 2007). The warming has been larger over land areas than over the oceans. In the northern hemisphere, the warming has been largest during winter and spring. In the boreal zone, the annual mean temperatures have warmed

J. Räisänen (✉)
Department of Physics, University of Helsinki, P.O. Box 48,
00014 University of Helsinki, Helsinki, Finland
e-mail: jouni.raisanen@helsinki.fi

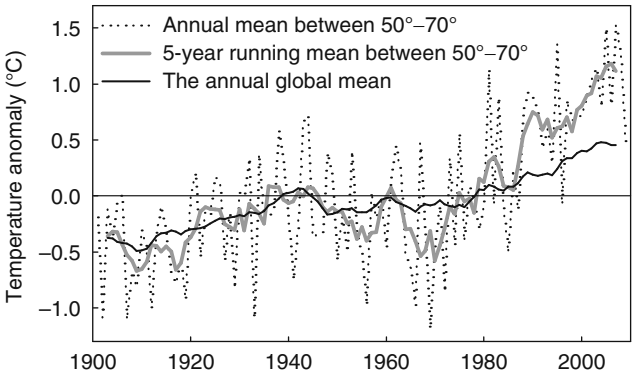

Fig. 8.12 Observed variations in temperature between the years 1901 and 2009. The *dotted line* shows annual temperature anomalies (i.e. differences from the mean value of 1961–1990) averaged over the land areas between 50 and 70°N and the dashed grey line their 5-year running mean. The 5-year running global mean temperature anomalies are shown by a *solid black line*. The data are from NCDC (Smith and Reynolds 2005)

more than in the global mean (Fig. 8.12). The twentieth-century warming has occurred in three phases: warming until the 1940s, followed by a slight cooling and a rapid warming from about the 1970s.

In the boreal zone (land areas between the latitudes 50 and 70°N), mean temperature during the period from May to August (hereafter MJJA) has increased in a similar three-phase behaviour as the annual mean temperature. When expressed as a linear trend, the warming since the beginning of the twentieth century has been about the same as the global annual mean warming (0.07°C/decade or 0.8°C in total). However, the warming since the mid-1970s has been much faster, nearly 0.3°C/decade for the period 1976–2009. Although linear trends depend on the period used in calculation, they allow an easy way to characterise spatial differences. From Fig. 8.13a, b, it can be seen that the warming from the beginning of the twentieth century has not been spatially uniform. There are some limited regions in the boreal zone that show no warming or may even have cooled, but the vast majority of the boreal area shows an increasing temperature trend over the period 1901–2009. The largest positive trends are about +1.5°C per century.

Since the 1970s, MJJA temperature trends are characterised by widespread warming (Fig. 8.13c, d). In parts of Europe and Siberia, the warming has been 0.5–0.7°C per decade, whereas some regions in North America have cooled slightly. Changes in atmospheric circulation modify the regional temperature trends, and natural climatic variability affects the statistical significance of the trends. A majority of the positive trends in Fig. 8.13a are statistically significant at 5% level, but due to the large natural variability and the short time period, just the largest trends in Fig. 8.13c are statistically significant. One clear implication of temperature increase is the lengthening of the growing season which can be seen as advanced bud burst of European rowan (*Sorbus aucuparia*) (Sect. 4.2.6).

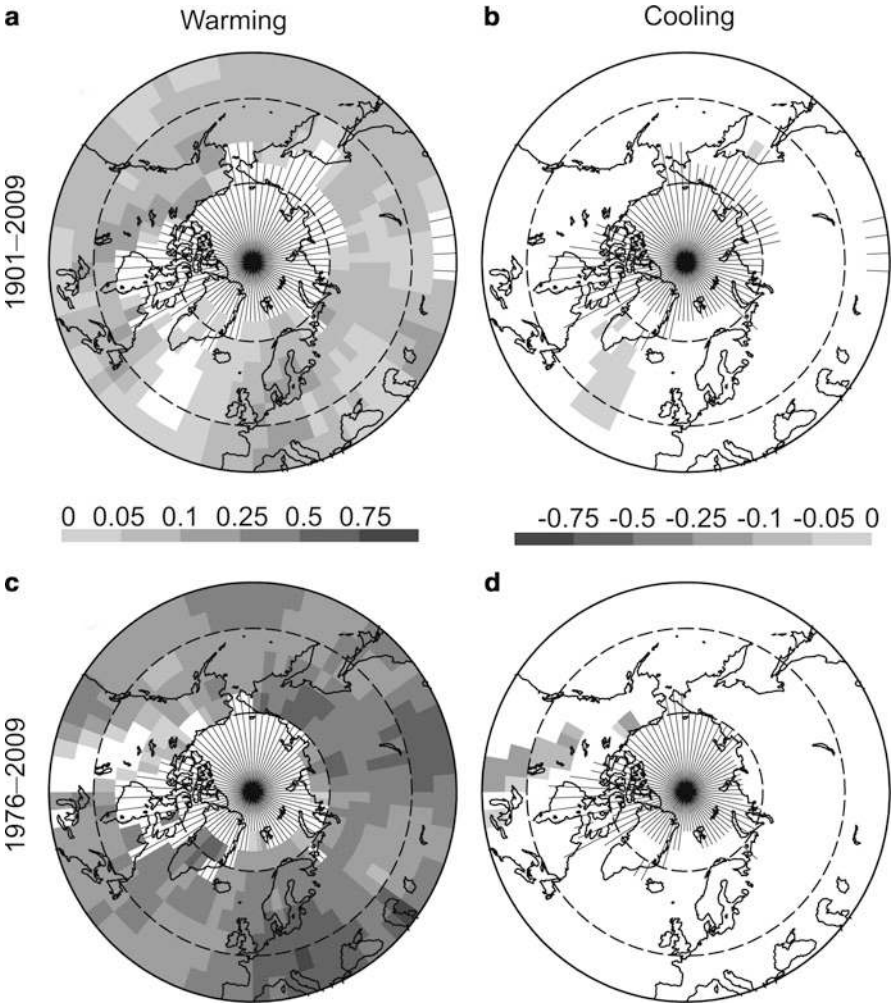

Fig. 8.13 Linear trends of MJJA temperatures (°C/decade) for (**a**)–(**b**) 1901–2009 and (**c**)–(**d**) 1976–2009. Areas with warming are shown in (**a**) and (**c**), areas with cooling in (**b**) and (**d**). Areas with missing data are indicated with north–south-oriented lines. The data are from NCDC (Smith and Reynolds 2005)

Effects of urbanisation on the land-based temperature record are negligible as far as hemispheric- and continental-scale averages are concerned because the very real but local effects are avoided or accounted for in the data sets. Trenberth et al. (2007) estimate the error due to urbanisation to be less than 0.01°C/decade (best estimate 0.006°C/decade) over land areas. Similarly, there may exist some random like error sources, like changes in observation sites, that tend to cancel out when averaging is done.

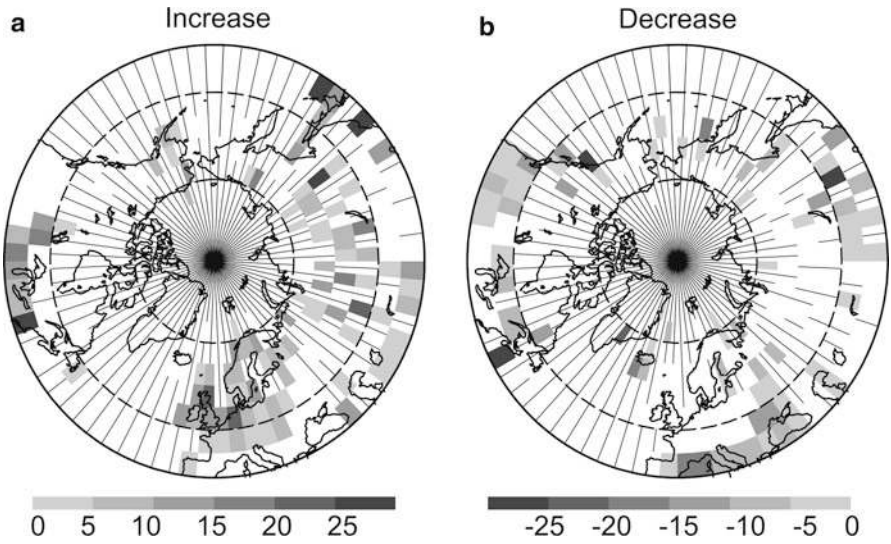

Fig. 8.14 Linear trends of MJJA precipitation sum (mm/decade) for the years 1976–2009. Areas with increasing precipitation are shown in (**a**) and areas with decreasing precipitation in (**b**). Areas with missing data are indicated with north–south-oriented lines The data are from NCDC (Smith and Reynolds 2005)

Area-averaged temperature variations and changes are known with good accuracy during the twentieth century. However, precipitation variations are known with spatially varying accuracy. There are two basic difficulties that cause inaccuracies to precipitation estimates. Firstly, measurements of precipitation suffer from undercatch due to wind and other error sources. Local conditions have a large effect on the measured amount, so any changes, for example, in wind exposure or improvements in the instrument, may break the homogeneity of measurement series. Secondly, global data sets have too few stations to catch the large spatial variability of precipitation; thus, in some regions of the world, the sample is too small to cover the spatially complex phenomena. For these reasons, precipitation trends are known less accurately than temperature trends.

There are several global land precipitation data sets, but they do not show consistent long-term trends over global land areas (Trenberth et al. 2007). In the NCDC data set used in this book, boreal zone annual, as well as MJJA, precipitation shows some increase during the twentieth century (Peterson and Vose 1997). However, the changes have varied in sign within the boreal zone (Fig. 8.14). In most parts of Eurasia, including northern Europe, MJJA precipitation has increased since the 1970s, but there have also been some areas with decrease. In North America, increasing and decreasing trends have been more in balance. From spatially detailed analysis it is known that the pattern of changes can be more complex than shown in Fig. 8.14. For example, the increase in northern Europe breaks into regions of

increase and decrease in a more detailed analysis (BACC Author Team 2008). Due to large natural variability, regional trends may lack coherence, and trend analysis is sensitive to selection of the time period.

The moisture holding capacity of the atmosphere increases at a rate of about 7% per °C. Temperature increase alone may therefore alter the hydrological cycle, especially the characteristics of precipitation (amount, frequency, intensity, duration, type). A warmer climate is expected to increase the risk for both drought and floods. Furthermore, changes in precipitation characteristics are complicated by aerosols that affect cloud formation processes. The changes in water that is available for the trees, that is, soil moisture, are determined by changes in precipitation, evapotranspiration and run-off. There are studies utilising observations and model calculations (e.g. Dai et al. 2004; Huntington 2006; Groisman et al. 2007), but a comprehensive view of changes in soil moisture conditions is lacking in the boreal zone.

Intensification of westerlies since the 1960s has increased air flow from oceans to continents, and its effect on precipitation and temperature anomalies can be seen during the winter half-year (Trenberth et al. 2007). Although the most notable climatic changes in the boreal zone have occurred during the winter and spring seasons, some of these changes also affect conditions at the beginning of the growing season that has shifted earlier (Sect. 4.2.6). Snow-covered area has declined in the northern hemisphere, and the reduction has been largest during the months of March and April (Lemke et al. 2007a, b). Earlier snowmelt occurs near the edges of the snow-covered area, thus lengthening the period of evaporation from soil and increasing the risk for drought. In April, the northern hemisphere snow cover extent is strongly correlated with the 40–60°N April temperature reflecting the feedback between snow and temperature.

As noted in the previous subsection, the concentration of greenhouse gases and aerosols has increased markedly during the industrial period. The globally averaged net radiative forcing since 1750, due to both human-induced warming and cooling effects, is estimated to be $+1.6$ W m^{-2}, with uncertainty range from $+0.6$ to $+2.4$ W m^{-2} (Forster et al. 2007). Hegerl et al. (2007) conclude that most of the observed increase in global mean temperature during the last 50 years is very likely due to the increase of anthropogenic greenhouse gas concentrations. However, in the boreal zone, natural climatic variability is large, and modes of variability such as the Arctic Oscillation (or its 'European' manifestation, the North Atlantic Oscillation) provide large regional differences in the observed climatic changes.

8.3.3.1 Global Climate Models

The primary tool used for understanding past climate changes and making projections of future climate change are three-dimensional global climate models (GCMs), also known as general circulation models. These models attempt to explicitly simulate the main physical phenomena that affect atmospheric weather and ocean circulation, land surface conditions and the state of sea ice and snow cover. The

models are built on well-known hydrodynamic and thermodynamic principles that describe the conservation of mass, water, energy and momentum within the climate system, rather than, for example, empirical correlations between temperature and greenhouse gas concentrations. The basic equations used in atmospheric models, that is, two equations for the horizontal wind components, the thermodynamic equation, the hydrostatic balance equation, the continuity equation, and conservation equations for water vapour and other trace substances, were given in the Box 8.1. A similar set of equations is also used in ocean models, with the main difference that the equation for water vapour is replaced by an equation for salinity. This solid physical basis gives a strong reason to think that these models are useful tools for exploring the behaviour of the climate system and its response to changes in external forcing such as increases in greenhouse gas concentrations.

On the other hand, limitations in computing power make it impossible to represent the full complexity of the real world in any model. This, together with the uncertainty associated with future greenhouse gas and aerosol emissions and natural climate variability, makes it impossible to give exact predictions of future climate.

The atmospheric components in current GCMs typically have a grid spacing of 200–300 km in the horizontal direction. In the vertical direction, there are typically about 30 levels between the surface and the model top at 30–50-km height, the spacing of levels increasing from a few hundred metres in the boundary layer to several kilometres in the stratosphere. Resolution of the oceanic model components is similar or slightly better. Phenomena acting on scales smaller than the grid spacing cannot be resolved explicitly. The impact of these phenomena needs to be parameterised, that is, estimated indirectly from the grid-scale conditions simulated by the model.

The most important parameterised phenomena in the atmospheric components of climate models include the transfer of solar and thermal radiation, small-scale mixing in the atmospheric boundary layer, vertical convection and, in particular, the formation of clouds and precipitation. The other model components, representing the ocean, sea ice and land surface, have their own parameterised phenomena, and parameterisations are also needed when describing exchange of heat, water and momentum between the atmosphere and other components. Some of the feedbacks that affect the magnitude and in some cases direction of climate changes are strongly sensitive to the parameterisation of sub-grid-scale phenomena, changes in cloudiness being the most notorious example.

In addition to the parameterisation problem, uncertainty in the results of climate models also arises from the neglect of some potentially important phenomena. For example, climate-induced changes in vegetation have this far been excluded in most model simulations, including those used in Sect. 8.3.3.2 below.

The atmospheric components of GCMs are, except for a coarser horizontal and vertical resolution, very similar to the models used in operational weather forecasting. The raw model output thus consists of daily or sub-daily time series of weather, for each grid point at the surface and higher in the atmosphere. Obviously, however, the daily evolution of weather is not predictable for several decades in

the future. Useful information in climate model output therefore resides in the statistical properties (long-term means, measures of variability, etc.) rather than in the daily details of simulation. For a sufficiently strong external forcing such as a large increase in greenhouse gas concentrations, the changes in these statistical properties become large enough to be discernible from the internally generated chaotic variability in the simulations.

GCMs have been developed and are used at a large number of research institutions. An intercomparison between the climate changes simulated by different models provides one way of estimating the uncertainty in future climate changes in the real world. However, this measure should be used with some care. While a disagreement between model simulations demonstrates that at least some of the models give unrealistic projections, an agreement between them does not necessarily prove that the models are right.

8.3.3.2 Projected Climate Changes for the Rest of the Twenty-First Century

Climate modellers often prefer to talk about projections rather than predictions or forecasts of future climate change. This is because the actual evolution of climate will be partly dependent on future human activities, in particular the magnitude of greenhouse gas and aerosol emissions. To characterise the uncertainty associated with emissions, a number of different emission scenarios have been developed. The most widely used set of these have been the IPCC (Intergovernmental Panel on Climate Change) SRES (Special Report on Emissions Scenarios) scenarios (Nakićenović and Swart 2000).

The SRES scenarios are based on alternative but plausible and internally consistent sets of assumptions about the demographic, socioeconomic and technological changes that together determine the evolution of emissions in the future. For a more detailed discussion of these underlying assumptions, the reader is referred to Nakićenović and Swart (2000). The scenarios remain reasonably similar in the early twenty-first century, for example, all of them include an initial increase in CO_2 emissions in the next few decades (Fig. 8.15). Towards the end of the century, the scenarios diverge, with some of them indicating a continuing rapid increase of greenhouse gas emissions driven by the increasing energy demand of the world, and others pointing towards a gradual decline in emissions allowed by reduced population growth, alternative energy sources and a shift towards a less energy-intensive economy. Nevertheless, the concentrations of the most long-lived greenhouse gases, particularly CO_2 and N_2O, keep rising even in those scenarios in which emissions are reduced. The best-estimate CO_2 concentration in the year 2100, as derived by an off-line carbon cycle model, varies from ca. 540–960 ppm between the lowest (B1) and highest (A1FI) SRES scenarios (Houghton et al. 2001), to be compared with the present-day concentration of 390 ppm.

Anthropogenic increases in atmospheric aerosol loading have suppressed greenhouse-induced warming during the twentieth century but will not necessarily

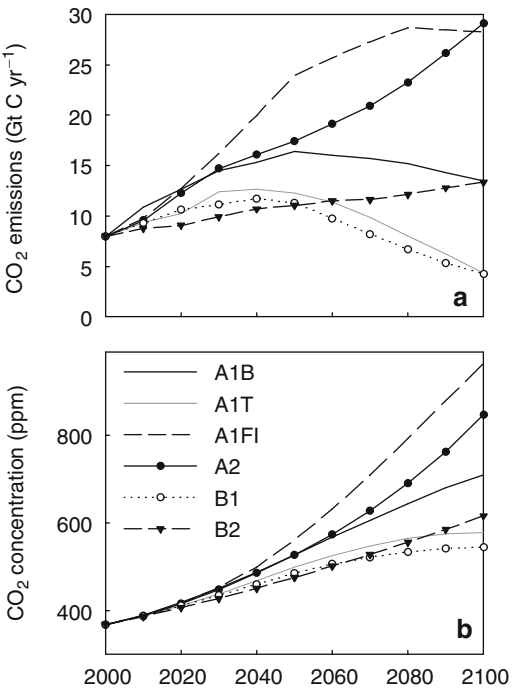

Fig. 8.15 CO_2 emissions (**a**) and the resulting best-estimate CO_2 concentrations (**b**) for the six SRES scenarios

continue to do so in the future. The main contributor to anthropogenic aerosol-induced cooling, SO_2 emissions, is still projected to increase in a global mean sense during the first decades of the twenty-first century in many SRES scenarios, which would suppress warming during this period. By the end of the century, however, the worldwide introduction of cleaner technologies is projected to reduce global SO_2 emissions well below present-day levels. Due to the very short lifetime of tropospheric aerosols, this would result in an immediate decrease in sulphate aerosol concentrations. Thus, greenhouse gas-induced warming is projected to become increasingly dominant over aerosol-induced cooling.

In its Fourth Assessment Report (Meehl et al. 2007), the IPCC estimates that the global mean warming that would occur during this century under the lowest SRES scenario (B1) would be within the range 1.1–2.9°C, with a best estimate of 1.8°C. The corresponding range for the highest scenario (A1FI) is 2.4–6.4°C, with a best estimate of 4.0°C. In both cases, the quoted uncertainty ranges take into account both the variation in warming under the same scenario of greenhouse gas concentrations between different GCMs and the uncertainty in modelling the feedback from climate change to the atmospheric CO_2 concentration. The within-scenario uncertainty associated with the modelling of feedbacks in the climate system is thus comparable with the differences between the lowest and highest emission scenarios. However, this should not obscure the fact that the magnitude of the warming will depend strongly on the magnitude of greenhouse gas emissions.

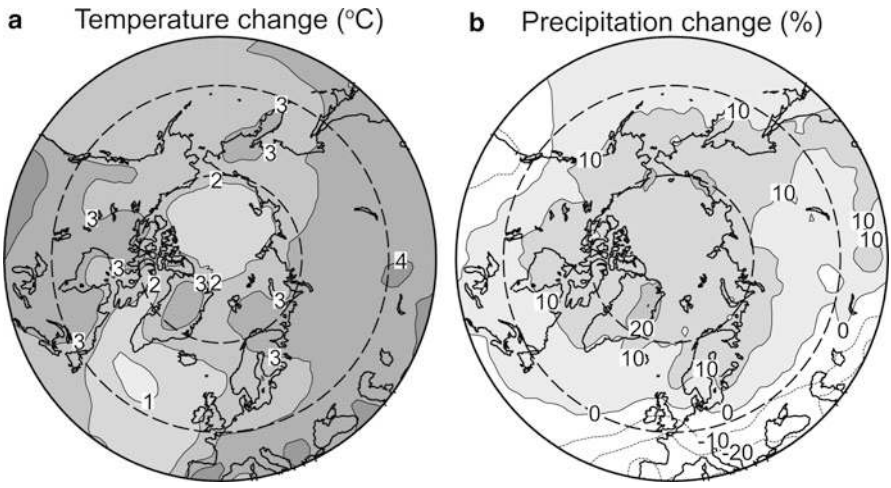

Fig. 8.16 Simulated changes in MJJA mean temperature (°C) (**a**) and precipitation (%) (**b**) from the recent past (1971–2000) to the late twenty-first century (2070–2099), as averaged over 21 climate models. All simulations are based on the SRES A1B emissions scenario. The two *dashed lines* show the latitudes 50 and 70°N

Thus, as mankind has little control of feedbacks in the natural climate system, our primary possibility to alleviate future climate changes is to reduce the emissions of CO_2 and other greenhouse gases.

Below, the typical features and uncertainties of GCM-simulated climate change are illustrated for the SRES A1B scenario, which is, in terms of greenhouse gas emissions, in the midrange of the SRES scenarios (Fig. 8.16). For example, CO_2 emissions are projected to approximately double by 2050, declining slightly thereafter, and CO_2 concentration is projected to rise approximately to 710 ppm by the year 2100. The analysis is based on the results of 21 recent GCMs contributing to the World Climate Research Programme 3rd Coupled Model Intercomparison Project (WCRP CMIP3, Meehl et al. 2007), and climate changes are calculated as differences between the mean values for the years 2070–2099 and 1971–2000. The focus is on the MJJA season that is most important for growth of boreal forests.

Maps of temperature and precipitation change, as averaged over the 21 models, are shown in Fig. 8.16. The average simulated warming in the boreal forest zone is slightly over 3°C, being comparable to but slightly higher than the 21-model annual mean global warming (2.6°C) in the same simulations. The warming is geographically relatively uniform but has, in this season, a tendency to increase from north to south. Precipitation is simulated to increase slightly in almost all of the boreal forest zone but with larger increases in the north than in the south. The opposite patterns of temperature and precipitation change may be physically related via the surface energy balance. The risk that warming would lead to a drying of the soil is larger in the southern areas where the increase in precipitation is smaller and, if the soil becomes sufficiently dry, then the ability of evapotranspiration to

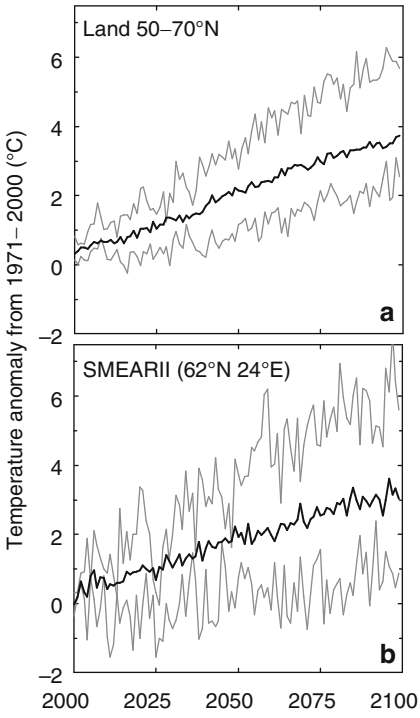

Fig. 8.17 Simulated time series of MJJA mean temperature, as averaged over all land areas at 50–70°N (**a**) and in an individual location (**b**). Temperatures are given as differences from the mean value in the years 1971–2000. In each case, the *central line* represents the mean of 21 climate models and the other *two lines* the individual models with the smallest and the largest warming

cool the surface will be reduced. Nevertheless, as illustrated by Figs. 8.17 and 8.18 below, the geographical variation of these simulated climate changes is relatively small when compared with the variation between individual models.

Climate is expected to warm gradually throughout the twenty-first century, although the warming is punctuated by substantial interannual variability (Fig. 8.17). The details of this variability are not predictable, and they are therefore largely smoothed out when averaging the temperatures over a large number of individual models. However, the differences in the rate of warming between individual models are also substantial and more so for individual grid boxes (Fig. 8.17b) than for averages taken over the whole boreal zone (Fig. 8.17a). Still, all models simulate some warming in practically the whole boreal forest zone.

For precipitation, the signal-to-noise ratio between the simulated anthropogenic climate change and natural variability is much lower than for temperature (Fig. 8.18), particularly when we consider the evolution of climate on the scale of individual grid boxes. Anthropogenic changes in precipitation are thus likely to become more slowly discernible from natural variability than changes in temperature. The variation between the individual models is also larger for precipitation than for temperature changes. Nevertheless, in most parts of the boreal forest zone, a large majority of the models agree on a long-term increase in precipitation.

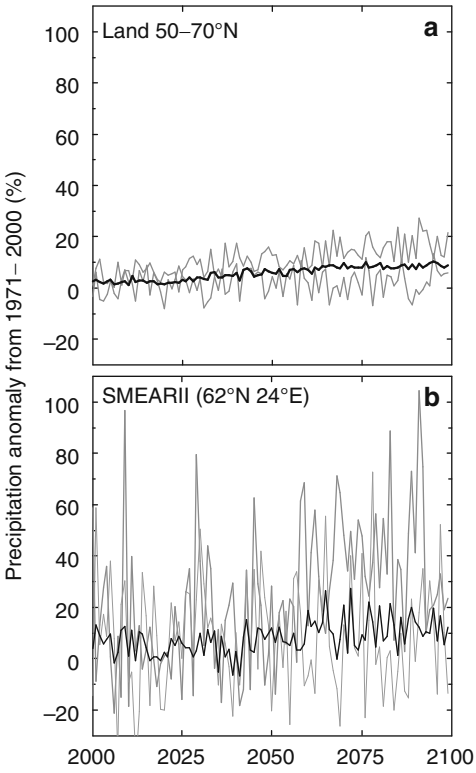

Fig. 8.18 As Fig. 8.17, but for changes in precipitation

8.3.3.3 Acknowledgments

We acknowledge the modelling groups for making their model output available for analysis, the Program for Climate Model Diagnosis and Intercomparison (PCMDI) for collecting and archiving these data and the WCRP's Working Group on Coupled Modelling (WGCM) for organising the model data analysis activity. The WCRP CMIP3 multi-model data set is supported by the Office of Science, US Department of Energy.

8.3.4 Responses of Forest Ecosystems to Climate Change

Pertti Hari, Jaana Bäck, and Eero Nikinmaa

There are several changes in the metabolic processes of trees caused by the climate change. These responses have to be converted to stand level to achieve

P. Hari (✉)
Department of Forest Sciences, University of Helsinki, P.O. Box 27,
00014 University of Helsinki, Helsinki, Finland
e-mail: pertti.hari@helsinki.fi

an understanding of the expected changes in boreal forests. For example, the photosynthetic rate can be assumed to accelerate due to the increased availability of CO_2. Is the growth increased in the same way as photosynthesis or are there internal feedbacks in a tree or in forest ecosystems that modify the response? The ecosystem model MicroForest (Chap. 7) combines several processes and regularities in tree structure to produce a prediction of ecosystem development, with important insights into the responses of boreal forest ecosystems.

The increasing atmospheric CO_2 concentration increases maximum photosynthetic rate and increases the annual amount of sugars available for growth and metabolism. The annual amount of photosynthesis in unshaded conditions is a key parameter in the model MicroForest. This fact opens a possibility to introduce the effect of increasing CO_2 concentration on photosynthesis into model simulations.

We analysed the effect of increasing CO_2 concentration on stand development with SMEAR II stand. The basic run in the in Chap. 7 assumes implicitly stable CO_2 concentration. For comparison, we introduced the effect of increasing CO_2 by assuming that the parameter values are estimated at 380 ppm, that is, this concentration is the reference CO_2, and we assumed a linear relationship between maximum photosynthesis and the atmospheric CO_2 concentration. The simulated stand photosynthesis had, as expected, a clear increasing trend (Fig. 8.19a). In contrast, the simulated stand volume reacted very weakly to the accelerated photosynthesis (Fig. 8.19c): the stand volume was even smaller at the end of the simulation than without increasing CO_2 concentration. This result is caused by the change in allocation to favour roots. As only CO_2 concentration was modified, the release of nitrogen from proteins in soil by microbes did not change and annual nitrogen uptake remained stable. The trees were unable to produce additional functional substances, and this is why the response of the stand to elevated CO_2 is very small. The model assumes no acclimation in foliar nitrogen content. If trees were to acclimate their leaf nitrogen content to the availability of nitrogen, the growth of trees would also have reacted along increasing atmospheric CO_2 concentration.

The expected temperature increase has two effects: it prolongs the metabolically active season and accelerates decomposition of soil organic matter. Extension of the active season increases annual photosynthetic production, and its effects are rather similar to those obtained for increasing CO_2 concentration, that is, the effect is quite small if it is not associated with increased nitrogen uptake from soil.

The decomposition of soil organic matter is slow in boreal forests since the pools of proteins—lignin, cellulose and lipids—are over tenfold when compared with the annual litter input. The model MicroForest has a special sub-model for decomposition of soil organic matter. The value of the parameter b_{1n} in Eq. 7.25 determines the decomposition rate of proteins in the simulations. The effect of increasing temperatures on stand growth was introduced by assuming that the dependence of the value of the parameter b_{1n} for temperature increase ΔT is

$$b_{1\,n}(\Delta T) = {q_{10}}^{\Delta T}\, b^0_{1\,n}, \tag{8.10}$$

where q_{10} is parameter and b^0_{1n} is the parameter value used in the Chap. 7.

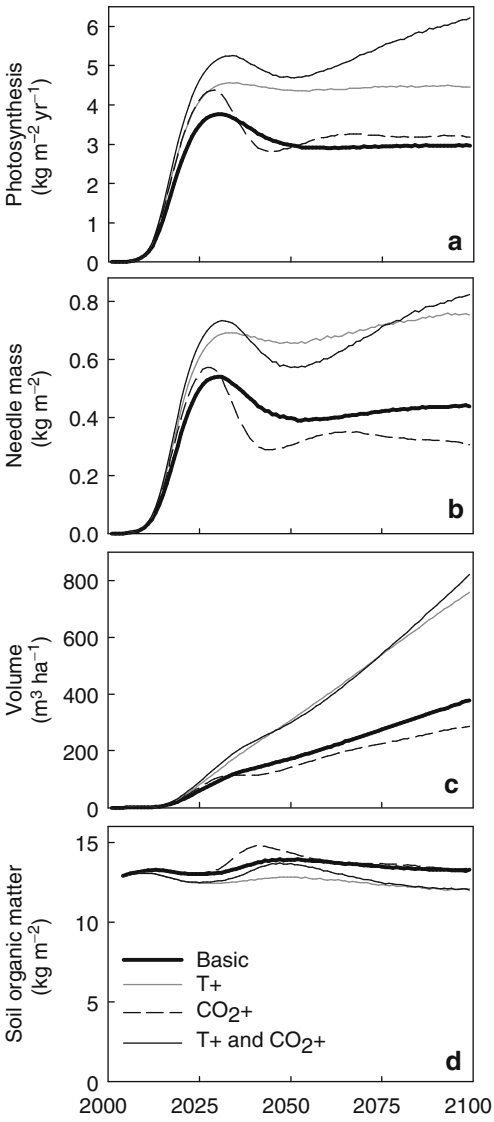

Fig. 8.19 Simulated photosynthesis (expressed in units of sugars) (**a**), needle mass (**b**), volume (**c**) and mass of soil organic matter (dry weight) (**d**) by MicroForest for the years 2000–2100 with different scenarios: no change in temperature or atmospheric CO_2 concentration, increase in temperature (0.4°C/decade), increase in CO_2 concentration (1.5 ppm year^{-1}) and increase both in temperature and CO_2 concentration

Temperature records show warming in southern Finland, although the interannual variation nearly hides the signal. We assumed that temperature will increase 0.4°C/decade which is a higher than the IPCC estimate of warming in the boreal zone. When this temperature increase is combined with the dependence of the value of the parameter on temperature, we get the result that decomposition of soil organic matter will be 20% faster in the year 2020 than in the year 1980 and 70% faster in the year 2100.

The simulations assuming accelerated decomposition of soil organic matter due to temperature increase indicated a strong response. The needle mass increased 70% at the end of the simulation in the year 2100 (Fig. 8.19b) and the annual photosynthetic production of the stand reflected the increase in needle mass (Fig. 8.19a). Annual wood increment responded also strongly (Fig. 8.19c). The increased availability of nitrogen in the soil due to accelerated decomposition of proteins in soil generates these large responses in simulations.

The increasing decomposition of soil organic matter generated large responses in the simulations. It is surprising that changes in the pools of soil organic matter are small, having only a very small declining trend (Fig. 8.19d), quite differently from the prediction of earlier models (e.g. Cox et al. 2000). The accelerated decomposition of proteins in soil enables a clear increase in nitrogen uptake and synthesis of functional substances, especially for leaves and fine roots. The accelerated decomposition is compensated to a great extent by the increased litter input on the soil. Thus, the weak response of soil organic matter can be explained by the compensating effect of increased litter fall.

When the accelerated decomposition due to the temperature increase and increasing CO_2 concentration were combined in the simulation, still larger responses were obtained. The needle mass increased 90%, photosynthesis 110% and stand volume 120%. The large organic molecules in the soil decreased by 10%. This small decrease can be explained with increased litter input that compensates for the faster decomposition. The strong response can be explained with high availability of nitrogen for the synthesis of functional substances and with accelerated photosynthesis due to increased availability of CO_2.

The annual increase in the release of ammonium from proteins in the soil is used to synthesise proteins in leaves, water transport system and fine roots. The lifetime of needles and fine roots is short, and thus nitrogen returns quickly into soil as proteins. In contrast, most of the woody structures endure for the whole lifetime of the trees, and proteins accumulate into woody structures. Thus, effectively, proteins are moved from soil into the pool of woody structures in trees. Since the annual release of nitrogen determines the fertility of the site (Sect. 7.3.3) and the protein concentration in wood is over one magnitude smaller than in soil, the increase in wood mass is about one magnitude larger than the loss in soil organic matter.

Anthropogenic nitrogen deposition is large in the south-western corner of European boreal forests; it can be over tenfold when compared with natural deposition. The leaching and evaporation of nitrogen are very small at SMEAR II (Sect. 5.6), and thus the nitrogen circulates efficiently within the ecosystem. The accumulation is, however, very slow; it can last for centuries. Magnani et al. (2007) reported clear relationship between nitrogen deposition and carbon fixation by ecosystems. Eddy Covariance measurements in stands forming chronosequences were used to obtain the net primary production. The material consists of 20 stands growing in Europe, Siberia and North America. Most of the stands are coniferous but four of them are deciduous. Scots pine is the dominating tree species on six sites (including SMEAR II stand). The analysis by Magnani et al. (2007) resulted in a clear relationship between nitrogen deposition and net primary production as shown in Fig. 8.20a.

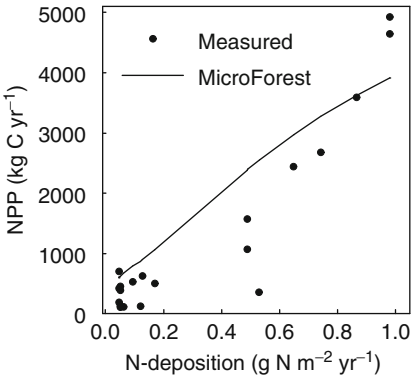

Fig. 8.20 Relationship between nitrogen deposition and net primary production. *Dots* indicate measured values reported by Magnani et al. (2007), and *line* indicates the response simulated with MicroForest

MicroForest is based on carbon and nitrogen fluxes in forest ecosystem, and nitrogen deposition is included as input flux in the ecosystem (Fig. 7.2). We simulate the effect of nitrogen deposition on net primary production with MicroForest using the site-specific nitrogen depositions as in the study by Magnani et al. (2007). We applied linearly increasing nitrogen depositions in such a way that at the end of the simulations at the age of 40 years, the deposition was as used in the study by Magnani et al. (2007). We also determined the net primary production of the stand as the annual increase in wood and soil organic material mass at the end of the simulations. The simulated relationship between nitrogen deposition and net primary production is rather close to that reported by Magnani et al. (2007). However, the shape of the relationship is different, since in the original study the regression is nonlinear and simulations result in linear relationship. The nitrogen impact reported by Magnani et al. (2007) has been argued to be too large. The simulations would, however, suggest that slowly increasing deposition and accumulation into the ecosystem might bring about the observed pattern.

8.3.5 Response of Boreal Forests to Climate Change

Pertti Hari, John Grace, Liisa Kulmala, Federico Magnani, Eero Nikinmaa, Twan van Noije, Jukka Pumpanen, Jouni Räisänen, David Stevenson, Timo Vesala, and Markku Kulmala

Boreal forests are versatile ecosystems, but there are, however, similarities among them. The most important similarity is that the processes are the same. All forests photosynthesise, take up nutrients, grow and finally die. Evidently, also the

P. Hari (✉)
Department of Forest Sciences, University of Helsinki, P.O. Box 27, 00014 University of Helsinki, Helsinki, Finland
e-mail: pertti.hari@helsinki.fi

regularities in the structure are based on water transport and nitrogen allocation. Thus, behind the versatile species, the same processes and structural regularities together with their dependencies on environmental factors govern the flows of material and energy within forests and between forest and the atmosphere. We urgently need understanding of the changes in the material and energy fluxes in forests because the forest soils contain large pools of carbon that may be released into atmosphere with climatic warming.

The boreal forests cover a huge area between 50 and 70°N: their total area is about 1.66×10^9 ha. There are several species forming stands, and the variation in fertility and the length of growing season is large. On the other hand, we have available very detailed information from one stand (SMEAR II) and dynamic model (MicroForest), based on carbon and nitrogen flows and structural regularities, tuned to the SMEAR II stand and tested with stands at the southern border of boreal forests. We need urgently to understand the effects of climate change on boreal forests. Thus, the question arises, can we apply the model MicroForest to all boreal forests?

We are facing two unpalatable alternatives, either we introduce strong assumptions and apply MicroForest or we state that it is premature to say anything about the behaviour of boreal forests under climate change. We think that valuable insights can be gained when applying MicroForest on all boreal forests even though the analysis is rough. The analysis should be tested with new material, and the detected shortcomings should be improved. In this way, we can improve our understanding in the long run. The other alternative is a blind alley and will not result in progress in the field.

Boreal forest has most tendency of all forests to grow as even-aged stands. They are 'born' after some catastrophe, such as clear cut, fire or storm, and they develop until a new catastrophe occurs, often at a rather high age of the stand. The natural fire cycle for the boreal biome is estimated to be approximately 100–150 years (Gauthier et al. 1996). The rotation period in forestry is about 100 years. Also more complicated stand structures exist, but we do not consider them in this first approximation of the changes in the carbon pools in boreal forests.

Boreal forests include several carbon storages that are relevant in the connection of climate change. Let $M_B(t)$ denote the amount of a carbon component in boreal forests as a function of time t and $F_B(t)$ the flow of a compound between the boreal-forests and the atmosphere. The component can be needle mass, amount of wood, amount of proteins, lignin, cellulose, lipids and starch in soil and the flow of CO_2, VOCs or N_2O. Changes in these masses or flows reflect the response of boreal forest to climate change. Let $M_S(t,\ \tau_S)$ denote the masses in a stand at stand age τ as a function of time and $F_S(t,\ \tau_S)$ the fluxes correspondingly. If the boreal forests are formed by even-aged stands, then we can approximate the masses and fluxes by summing the stand-specific values over the whole area. Thus,

$$M_B(t) \approx \sum_{\tau_S=1}^{\infty} A(t, \tau_S)\ M_S(t, \tau_S) \tag{8.11}$$

$$F_{\mathrm{B}}(t) \approx \sum_{\tau_{\mathrm{S}}=1}^{\infty} A(t, \tau_{\mathrm{S}})\ F_{\mathrm{S}}(t, \tau_{\mathrm{S}}), \tag{8.12}$$

where $A(t, \tau_s)$ is the area of stands having age τ_s in the boreal forests as a function of time t.

We can obtain approximation for any of the masses $M(t, \tau_s)$, at moment t and age τ_s from simulations with MicroForest. The development of the areas of stands at a given age through the centuries is difficult to obtain. This problem can be avoided by assuming that all stands have the same maximum age, often called as rotation time, and that the areas of each stand age classes are the same. Let τ_{R} denote the rotation time. Then we get

$$M_{\mathrm{B}}(t) \approx \sum_{\tau_{\mathrm{S}}=1}^{\tau_{\mathrm{R}}} \frac{A_{\mathrm{B}}}{\tau_{\mathrm{R}}} M_{\mathrm{S}}(t, \tau_{\mathrm{S}}) \tag{8.13}$$

$$F_{\mathrm{B}}(t) \approx \sum_{\tau_{\mathrm{S}}=1}^{\tau_{\mathrm{R}}} \frac{A_{\mathrm{B}}}{\tau_{\mathrm{R}}} F_{\mathrm{S}}(t, \tau_{\mathrm{S}}), \tag{8.14}$$

where A_{B} is the total area of boreal forests.

The boreal forests cover a huge area on the northern hemisphere, and the climate change varies within it. The spatial variation in the atmospheric CO_2 concentrations is really small, even the variation within years is larger. The temperature increase has some geographical features that we should introduce into our analysis. The nitrogen oxides have a rather short lifetime in the atmosphere, and they deposit within thousands kilometres from the emission source. This gives a clear geographical deposition pattern since the emissions are strongly concentrated into the industrialised centres in Europe, North America and eastern Asia. We consider that the boreal forests cover the land area between 50 and 70°N, and we divide this area in east–west direction into six zones each of them covering 60°. In this way, we obtain the following areas: Europe, Central Asia, eastern Asia and western, central and eastern North America.

We used the CO_2 concentrations from the SRES A1B emissions scenario, as tabulated in Appendix II.2 of Houghton et al. (2001) and averaged over the ISAM and BERN-CC reference simulations.

We derived the estimates for the twenty-first-century temperature changes in the May–June–July–August (MJJA) season from the SRES A1B climate change simulations included in the Third Coupled Model Intercomparison Project (CMIP3) data set (Meehl et al. 2007). We averaged geographically these changes over land grid boxes in the zone 50–70°N, dividing both North America and Eurasia to three longitude bands. The resulting temperature changes in the twenty-first century are 2.8°C in western, 3.2°C in central, and 3.0°C in eastern North America and 2.9°C in western, 3.5°C in central and 3.0°C in eastern Eurasia. We assumed

that the temperature increase started in the year 1965, which is in agreement with measurements (Smith and Reynolds 2005), and it will continue during the twenty-first century according to the scenarios.

We estimated nitrogen deposition to boreal forests in each of the above regions for the time period 1960–2000 using results from the TM4 chemistry-transport model, driven by meteorological data from ERA-40 (European Centre for Medium-Range Weather Forecasts Re-Analysis), as part of the RETRO (REanalysis of the TROpospheric chemical composition over the past 40 years) project (Schultz et al. 2007). Changes in the magnitude and spatial distribution of all the major anthropogenic and natural emissions of oxidised and reduced nitrogen compounds are the main drivers of trends in nitrogen deposition. Prior to 1960, we extrapolate backwards in time using decadal emission estimates from the EDGAR-HYDE data set (van Aardenne et al. 2001), which spans 1890–1990. We calculated for each region, the ratio of the 1960s mean nitrogen deposition from TM4 to the mean 1960s EDGAR-HYDE emissions; we used obtained value to scale the emissions for earlier decades. Prior to 1890, deposition rates were assumed to remain at their 1890s values. Future levels of nitrogen deposition strongly depend upon future emissions and in particular the strength and level of implementation of air quality legislation (Dentener 2006). Here, we assume deposition remains constant beyond 2000.

We assume that the material and energy fluxes in boreal forests will respond to climate change as described in MicroForest, and we apply MicroForest to all boreal forests. In addition, we normalise the results in such a way that the biomass is 4.2×10^7 g ha^{-1} in a year in which the value has been measured for boreal forests in North America (Botkin and Simpson 1990). We analyse the responses of boreal forests to increasing CO_2 to nitrogen deposition and to accelerated decomposition due to temperature increase.

There are rather large differences in the nitrogen deposition between the six areas in boreal forests. Nitrogen deposition is largest near the big industrialised centres and moderate in the central North America and Siberia. The expected temperature increase has more even spatial distribution; the expected increase at 2100 varies from 2.8 to 3.5°C. The winds in the atmosphere mix the emitted CO_2 so effectively that the spatial concentration differences are minimal, and they do not generate spatial features in the responses of boreal forests.

We extended the simulations with MicroForest to cover boreal forests over the period 1750–2100. The nitrogen deposition increases carbon sequestration per hectare over two fold in western Eurasia when compared with east North America. The area of high nitrogen deposition in boreal forests is, however, so small that it reduces the importance of nitrogen deposition in the boreal scale.

When only CO_2 concentration changes in the simulations, then the response begins in the late nineteenth century, accelerates slowly tree growth during the twentieth century and rapidly declines after the year 2000 (Fig. 8.21a). The growth decrease in simulations is caused by accumulation of nitrogen in the soil and the shift in allocation from leaves to roots.

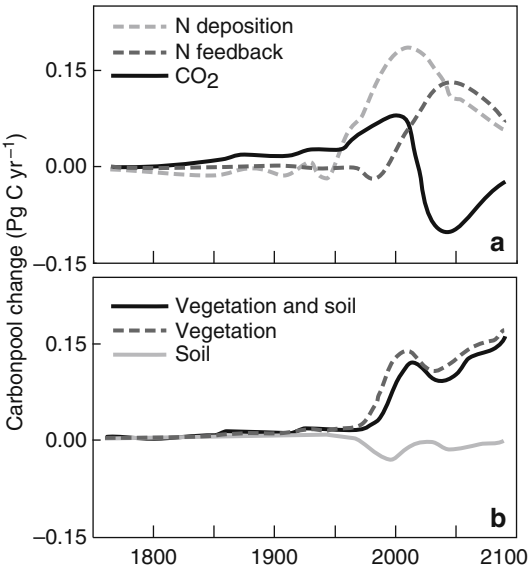

Fig. 8.21 Simulated changes in carbon pool of boreal forests as response to single changing factor (**a**) and as a response to temperature and CO_2 increase (**b**)

Changes in nitrogen availability and the CO_2 increase have strong interaction in carbon sequestration and the response cannot be derived from the single factor simulations. The trees can utilise effectively the additional sugars caused by enhanced photosynthesis associated with increased atmospheric CO_2 concentration to the synthesis of cellulose, lining and lipids for cell walls and membranes when simultaneously enhanced nitrogen availability, either due to accelerated decomposition of proteins or to nitrogen deposition, provides material for protein synthesis to construct the necessary enzymes and membrane pumps in the additional cells (Fig. 8.21b).

The large differences in nitrogen deposition generate geographical features in the responses of boreal forests to climate change. The sequestration increase is in western Europe having high nitrogen deposition, about twofold when compared with eastern North America (Fig. 8.22).

When we add together the responses of the six geographical areas we obtain the carbon sequestration in the boreal forests. According to our simulations, the carbon sequestration in boreal forests started at the beginning of the twentieth century, grew slowly, peaked in the beginning of the twenty-first century to 0.5 Pg (C) $year^{-1}$ and thereafter slowly declined (Fig. 8.23). Enhanced tree growth resulted in the accumulation of wood and other organic matter in boreal forests.

No data of the past carbon stocks in boreal forests are available, and we can only compare our simulations with other results dealing with northern forests around the year 2000. National forest inventories are based on large systematic samples of forest stands. The results provide reliable estimates of time series of several quantities describing forests in Finland. The Finnish forest inventories

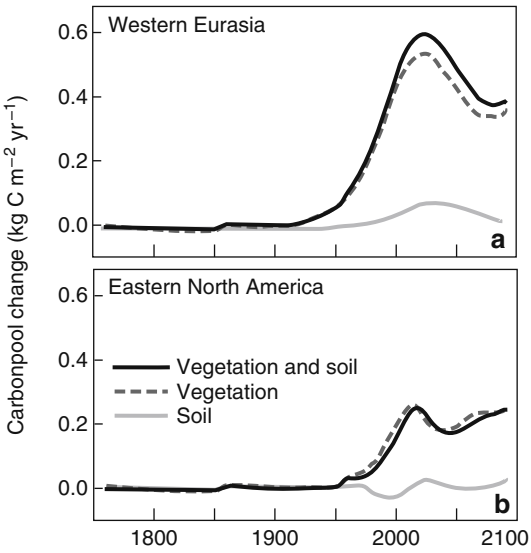

Fig. 8.22 Simulated changes in carbon pool in western Eurasia (**a**), a region of high anthropogenic nitrogen deposition and in eastern North America (**b**), a region of low anthropogenic nitrogen deposition

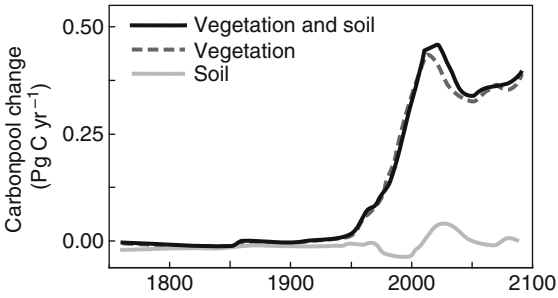

Fig. 8.23 Simulated changes in carbon pools of vegetation, soils and ecosystems in boreal forests during 1750–2100

indicate that annual growth increased from 50 to 100×10^6 m^3 $year^{-1}$ during the period 1950–2000. When the growth increase is converted from volume units to mass of carbon per unit area, we get 0.5 kg (C) m^{-2} $year^{-1}$. The simulations of carbon sequestration by vegetation for western Eurasia in the year 2000 result in 0.52 kg (C) m^{-2} $year^{-1}$, which is close to what is obtained in the Finnish national forest inventories. Drainage of peatlands, changes in forest structure and nitrogen fertilisation have all contributed to the forest growth increase in Finland. Thus, the simulated effect of climate change in carbon sequestration is evidently too large.

The analysis by Myneni et al. (2001) of temperate and boreal forests based on forest inventories and satellite images indicates carbon sequestration of 0.68 Pg (C)

year^{-1} by temperate and boreal forests during the period 1981–1999. The result obtained with MicroForest simulations for carbon sequestration by vegetation in boreal forests during the year 2000 is 0.5 Pg (C) year^{-1}. The analysed satellite images cover large areas south of boreal forests, and some northern boreal forests are evidently missing in the material. This discrepancy may explain the difference in the result obtained by Myneni et al. (2001) and simulations with MicroForest.

Stephens et al. (2007) estimated that the carbon sink of northern terrestrial areas in the year 2000 is 1.5 Pg (C) year^{-1} using measured atmospheric CO_2 concentrations and inverse modelling. But there is considerable uncertainty attached to this figure and the northern terrestrial area is rather poorly specified going much further south than in our simulation. Moreover, to obtain comparable results, the amount of wood cut and used in forestry has to be added to the 0.5 Pg (C) year^{-1} found in the MicroForest simulations. According to the official forest statistics by FAO (UN-ECE/FAO), the annual fellings of coniferous trees in the boreal region are 979 million cubic metres, equivalent to about 0.2 Pg (C) year^{-1}; thus, the simulated carbon sink in boreal forests is 0.7 Pg (C) year^{-1}, well within the uncertainty of the result of the inverse modelling.

Four different methods, national forest inventories, remote sensing, atmospheric inversion estimates and MicroForest model, have indicated strong carbon sink and sequestration into boreal forests. The magnitudes of the sink estimates are rather close to each other, although the areas are not exactly comparable with each other. The results based on direct measurements indicate the present situation, but the simulations with MicroForest have the additional advantage that they are able to predict the future carbon sequestration. Moreover, the simulations provide insights into the underlying biological causes. Processes in the boreal forests respond to the changes in the atmospheric properties generating changes in the flows in forest ecosystems. The accelerated decomposition of proteins in the soil, the increased nitrogen deposition from the atmosphere and enhanced photosynthesis due to elevated CO_2 concentration are able to amplify considerably the carbon sequestration in the boreal forests. The development of a simplified version of MicroForest and the introduction of it into GCMs (global climate models) will evidently improve our analysis.

Our results indicate that boreal forests responded strongly to climate change starting from the middle of the twentieth century. They will continue carbon sequestration in the coming decades if there are no increases in disturbance, for example, extensive outbreaks of insects or pathogens. The major influence seems to be through increased rate of nitrogen release from the soil organic matter due to temperature increase. The associated growth enhancement of vegetation seems to more than compensate for the net carbon release from the soil.

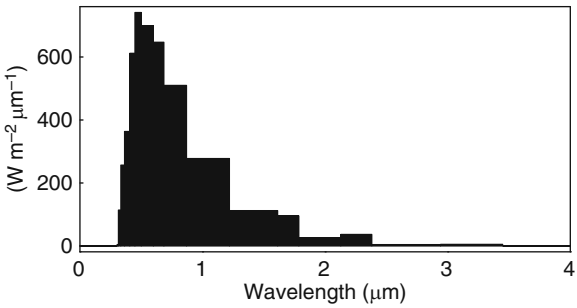

Fig. 8.24 Modelled 25-band spectrum of the radiation penetrating atmosphere, as used in calculating the surface albedo

8.3.6 Feedback from Forests to Climate Change

8.3.6.1 Climatic Effects of Increased Leaf Area: Reduced Surface Albedo and Increased Transpiration

Jouni Räisänen and Sampo Smolander

Green needles absorb strongly solar radiation and convert the radiation energy to heat. In contrast, snow reflects most of the radiation. The temperature increase in a forest stand will accelerate protein decomposition in the soil (Sect. 4.4) which can lead to better forest growth and increasing needle mass in the stand (Sect. 8.3.4). Thus, the increasing needle mass may generate positive feedback to climate change.

The increasing needle mass could result in several climatic feedbacks (Sect. 8.3.2). In this subsection, we focus on two of them: the impact of the leaf area change on surface albedo and its impact on transpiration. After a brief physical discussion of these feedbacks, their potential climatic importance is evaluated in simulations conducted with a state-of-the-art atmospheric general circulation model.

The spectral composition of the incoming below-atmosphere radiation and the spectral albedo of the surface determine the total albedo of a land surface. There are computer codes to determine the spectrum of incoming radiation (Freidenreich and Ramaswamy 1999; Stamnes et al. 1988, 2000). We assumed cloud-free subarctic winter atmospheric conditions (McClatchey et al. 1971) with a visible optical depth of 0.2 for continental aerosols and a solar zenith angle of 60°. The resulting spectra are shown in Fig. 8.24.

Computer models for (1) optical properties of single ice crystals and (2) for the scattering and reflection of light in a layer of snow[2] were used to determine

[2] Available from NASA GSFC FTP ftp://climate1.gsfc.nasa.gov/wiscombe/

J. Räisänen (✉)
Department of Physics, University of Helsinki, P.O. Box 48, 00014 University of Helsinki, Helsinki, Finland
e-mail: jouni.raisanen@helsinki.fi

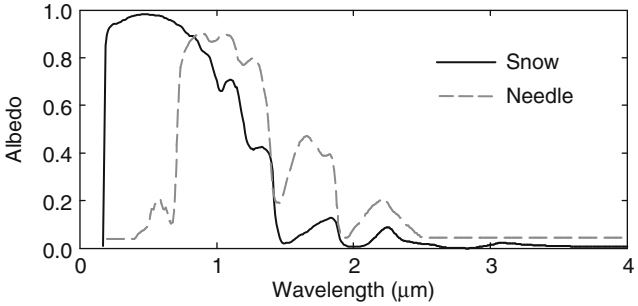

Fig. 8.25 Spectral albedo for snow and conifer needles

the spectral albedo of snow. The snowbed was modelled as an optically thick layer of spherical ice crystals (150 μm diameter). The resulting spectra are shown in Fig. 8.25. When calculating the snow-covered land surface albedo with these spectra, the result is 0.78, close to the value 0.8 used in the ECHAM5 model (Roeckner et al. 2003) as the maximum albedo of unvegetated snow-covered areas.

Coniferous needles absorb, reflect or transmit solar radiation. The energy of the absorbed radiation heats the needle. The LIBERTY model by Dawson et al. (1998) was used to model the fraction of incoming radiation that a needle absorbs, or reflects and transmits, at different wavelengths. The obtained needle spectral albedo is shown in Fig. 8.25. The needle has different albedo at different wavelengths, but if illuminated by the previously modelled skylight, its average albedo is 0.42 (calculated as a weighted average of the needle spectral albedo, with weights from Fig. 8.24), thus rather different from snow.

The spectrum of incoming skylight and the albedo spectrums for snow and conifer needles provide the necessary input to model the albedo of coniferous forests on a snow-covered ground. We used a two-stream canopy radiative transfer model by Ross (1981), modified for coniferous canopies as proposed by Smolander and Stenberg (2005). The model allows for the multiple scattering of radiation inside the forest canopy and between the canopy and the snow-covered ground. The canopy models account for the clumping of needles into coniferous shoots and the resulting effects for small-scale multiple scattering but exclude larger-scale structures (branches and tree crowns) typical of coniferous forest canopies. The lack of tree crowns is a somewhat unrealistic assumption, but in this case, we opted for simplicity. After several model runs for canopies with different leaf area index, the resulting canopy albedo as a function of canopy leaf area is shown in Fig. 8.26. As needles are non-flat objects, the coniferous canopy leaf (needle) area index was defined on a half of the total surface area basis (Chen and Black 1992).

All other factors being the same, transpiration from vegetation should be directly proportional to the transpiring surface area. Thus, for example, a doubling of leaf area should lead to a doubling of transpiration. In reality, this is a gross overestimate. This is because transpiration is limited by the availability of water and, in particular,

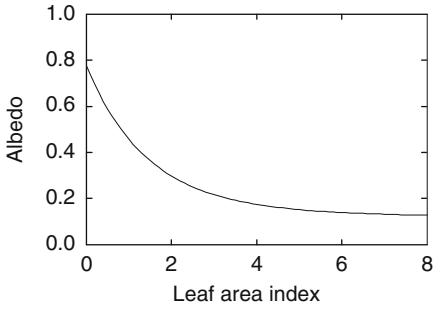

Fig. 8.26 Albedo of coniferous canopy on a snow-covered ground, as a function of canopy leaf area index

by the availability of energy. Furthermore, an initial increase in transpiration tends to increase boundary-layer relative humidity. This reduces the vapour pressure difference between plant stomata and the near-surface air, thus acting as a negative feedback to transpiration. On the other hand, any changes in transpiration may affect other aspects of the hydrological cycle, such as cloudiness and precipitation.

We conducted sensitivity experiments to estimate the impact of the leaf area albedo and transpiration feedbacks in more quantitative terms with the ECHAM5 atmospheric general circulation model (GCM) (Roeckner et al. 2003, 2006) coupled to a simple model of the upper ocean (Box 8.2).

Box 8.2

ECHAM5 is a state-of-the-art atmospheric GCM developed by the Max Planck Institute for Meteorology in Hamburg. For the simulations described here, ECHAM5 was run with a relatively low horizontal resolution (spectral truncation to total wave number 31, corresponding to a grid spacing of approximately 3.75° in latitude and longitude) and with 19 levels in the vertical. The atmospheric model was connected to a simple model of the upper ocean, consisting of a heat balance equation for a 50-m-thick water layer and a prognostic equation for sea ice thickness. To compensate for the lack of ocean currents in the thermodynamic ocean model, flux adjustments (Sausen et al. 1988) were used to keep sea surface temperatures near observed present-day values in the control simulation. An evaluation of the simulated present-day climate with observational data revealed a level of skill well comparable with other global climate models (Räisänen 2007). In a standard experiment with a doubling of the atmospheric CO_2 concentration, the model simulated a global mean warming of about 3°C, in good agreement with other models and the Intergovernmental Panel on Climate Change best estimate of climate sensitivity (Meehl et al. 2007).

In the ECHAM5 standard set-up, the evolution of leaf area follows a prescribed seasonal cycle based on the data set compiled by Hagemann (2002). The growing and dormant season values of leaf area are derived from ecosystem type classifications from the US Geological Survey (2001), and the seasonal cycle between these

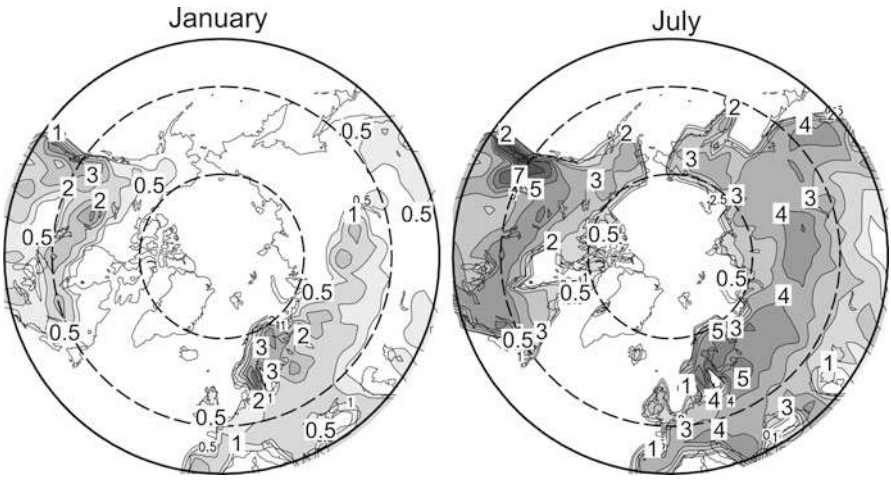

Fig. 8.27 Leaf area index (LAI) in the ECHAM5 control run in January and July

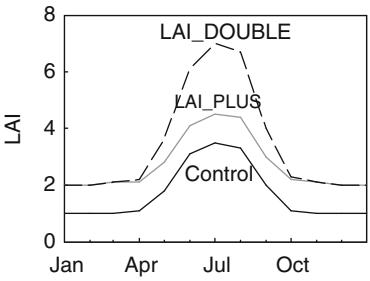

Fig. 8.28 Seasonal cycles of leaf area index (LAI) as averaged over the Eurasian and North American continents at latitudes 50–70°N, in the control simulation (CTRL) and the two sensitivity experiments LAI_PLUS and LAI_DOUBLE

extremes is based at high latitudes on observed monthly mean temperatures. In all months with an observed mean temperature of less than 5°C, leaf area retains its dormant season (winter) value (Fig. 8.27).

To study the sensitivity of the simulated climate to changes in leaf area, two 30-year model simulations with increased leaf area were made and compared with a control simulation (CTRL) with standard leaf area values. In one (LAI_PLUS), a seasonally invariant increase was added to the standard leaf area values at latitudes 50–70°N. The magnitude of this increase was such that the dormant season leaf area was doubled. In the growing season, the absolute increase was equally large, but the relative increase was smaller. In the other experiment (LAI_DOUBLE), leaf area was doubled in each month. All three simulations assumed the same near-present concentrations of greenhouse gases. The seasonal cycles of leaf area in the three simulations, averaged over the Eurasian and North American continents at latitudes 50–70°N, are shown in Fig. 8.28. Note that LAI_PLUS and LAI_DOUBLE are essentially identical from October to April so that they only differ from late spring to early autumn.

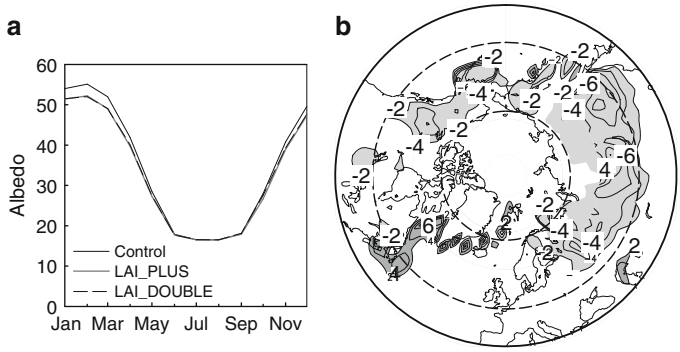

Fig. 8.29 Seasonal cycles of surface albedo, as averaged over the Eurasian and North American continents at latitudes 50–70°N, in the three simulations (**a**). The difference of surface albedo between the simulations LAI_PLUS and CTRL in February–March–April mean surface albedo (**b**). Contour interval 2%, zero contour omitted. *Light* (*dark*) shading indicates areas where the albedo has decreased (increased) by at least 2%

All three simulations were run for 30 years. To avoid eventual spin-up problems in the beginning of the simulations, the mean values shown here were calculated over the last 25 years.

The increase in leaf area affects the simulated climate in ECHAM5 by two primary mechanisms. First, it acts to reduce the surface albedo when there is snow on the ground. Second, it affects the calculation of surface fluxes, including the partitioning of available energy between sensible and latent heat fluxes. Other potential consequences of increased vegetation activity, such as changes in carbon cycle and in the production of biogenic aerosols, are not presented in these simulations.

The average seasonal evolution of the simulated surface albedo in the boreal forest zone is shown in Fig. 8.29a. Because leaf area only affects the albedo in ECHAM5 when there is snow on the ground, there is no difference between the three simulations in summer. In winter and early spring, the average surface albedo is about 3% lower in the simulations LAI_PLUS and LAI_DOUBLE than in CTRL. The geographical distribution of the difference of surface albedo between the simulations LAI_PLUS and CTRL during late winter and early spring (February–March–April) is shown in Fig. 8.29b. Because surface albedo is also affected by changes in snow and ice conditions, the changes are not exclusively limited to those areas where leaf area was increased.

Figure 8.30 shows the relative humidity, total cloudiness, precipitation and temperature differences in the simulations LAI_PLUS and CTRL and LAI_DOUBLE and CTRL, as averaged over the whole boreal forest zone at 50–70°N. The decrease in surface albedo shown in Fig. 8.29 acts to increase the amount of solar radiation absorbed at the surface in winter and spring (Fig. 8.31a). The increase is largest (on the average about 2 W m^{-2}) in March and April when there is much more solar radiation available than earlier in winter.

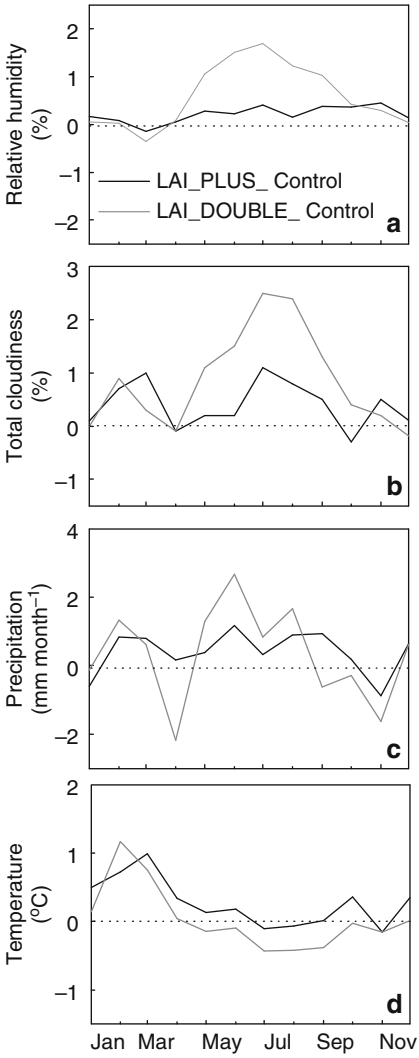

Fig. 8.30 Differences between the simulations LAI_PLUS and CTRL, and LAI_DOUBLE and CTRL in near-surface relative humidity (**a**), total cloudiness (**b**), precipitation (**c**) and surface air temperature (**d**), as averaged over the Eurasian and North American continents at latitudes 50–70°N

In summer, absorbed solar radiation decreases, particularly in the simulation LAI_DOUBLE, in which the increase in leaf area is largest. At the same time, there is an increase in thermal radiation (Fig. 8.31b), although this does not fully compensate the decrease in absorbed solar radiation. Both of these changes appear to be caused by increased cloudiness (Fig. 8.30b) that is most likely a consequence of the leaf area transpiration feedback.

Mean changes in the sensible and latent heat fluxes of the boreal forest zone are shown in Fig. 8.31c, d. For most of the year, the latent heat flux is larger in the simulations LAI_PLUS and LAI_DOUBLE than in CTRL. The sensible heat flux increases relative to CTRL in March and April but decreases in the summer,

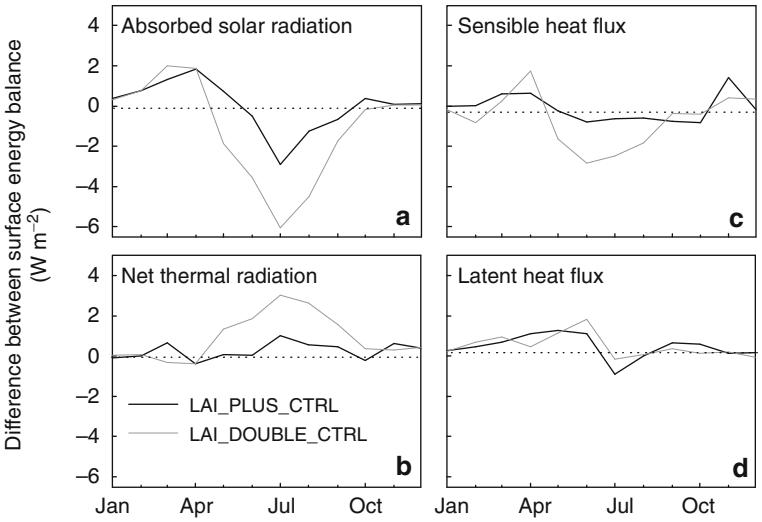

Fig. 8.31 Differences in surface energy balance (W m^{-2}) between the simulations LAI_PLUS and LAI_DOUBLE and the control simulation, as averaged over the Eurasian and North American continents at latitudes 50–70°N. Absorbed solar radiation (**a**), net (downwards minus upwards) thermal radiation (**b**), sensible heat flux (**c**), and latent heat flux (**d**)

particularly in the simulation LAI_DOUBLE. Thus, as expected, the increase in leaf area requires the model to consume a larger fraction of the available radiation energy to the latent heat flux at the expense of the sensible heat flux.

The increase in latent heat flux means an increase in evapotranspiration. However, the increase is relatively modest: in both simulations, LAI_PLUS and LAI_DOUBLE, the annual mean evapotranspiration is only 2% (6 mm year^{-1}) higher than in CTRL. The relative change is thus over an order of magnitude smaller than the change of leaf area applied in the experiments. This might partly result from compensation between increasing transpiration and decreasing surface evaporation; unfortunately, this cannot be verified because these two components are not separated in the ECHAM5 output. More importantly, evapotranspiration is limited by the availability of energy.

Another constraint to evapotranspiration is the availability of water. This factor likely limits the simulated increase in evapotranspiration in summer, particularly in the southern parts of the boreal forest zone.

The increase in evapotranspiration and the decrease in sensible heat flux (that reduces the heating of the lower atmosphere) together act to increase the near-surface relative humidity in summer, particularly in the simulation LAI_DOUBLE (Fig. 8.30a). On the other hand, moistening of the surface layer is one of the factors that limit the increase in evapotranspiration. The increase in relative humidity also leads to an increase in cloudiness in summer (Fig. 8.30b). Therefore less solar radiation reaches the surface (Fig. 8.31a), although this is partly compensated by an increase in the atmospheric counterradiation in the thermal part of the

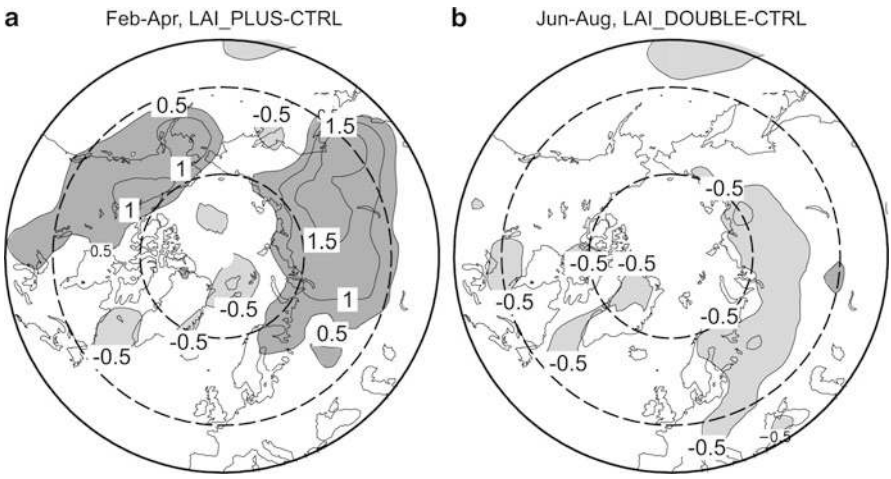

Fig. 8.32 Differences in surface air temperature between the simulations LAI_PLUS and CTRL in February–March–April (**a**) and between the simulations LAI_DOUBLE and CTRL in June–July–August (**b**). Contour interval is 0.5°C; zero contour is omitted. *Dark* (*light*) shading indicates areas where temperature has decreased (increased) by at least 0.5°C

electromagnetic spectrum (Fig. 8.31b). In summary, the changes in the hydrological cycle and in the surface energy balance are strongly interconnected.

The increase in LAI leads to a small overall increase (about 5 mm year^{-1}) of precipitation in the boreal forest zone (Fig. 8.30c). In the simulation LAI_DOUBLE, in particular, the largest increase occurs in summer.

The impacts of increased LAI on simulated surface air temperature are twofold (Figs. 8.30d and 8.32). From January to April, the temperature response is dominated by the decrease in surface albedo. Thus, temperatures are slightly higher in the simulations LAI_PLUS and LAI_DOUBLE than in the control simulation. The largest area mean warming of about 1°C occurs in March in the simulation LAI_DOUBLE and in February in the simulation LAI_PLUS. The warming is greatest in Siberia (Fig. 8.32a). By contrast, the summer mean temperature decreases slightly in most of the boreal forest zone, particularly in the simulation LAI_DOUBLE, at least in part due to the increase in cloudiness (Fig. 8.30b). However, the sign of the summertime temperature changes might be sensitive to the GCM-specific parameterisations of albedo and other surface properties. In an early model study by Bonan et al. (1992), a total removal of boreal forests also led to a cooling in summer, resulting from a much later snowmelt in spring. More recently, Betts et al. (2007) simulated a pronounced cooling in spring but mostly small temperature changes in summer due to historical conversion of North American and Eurasian forests to agricultural land.

Acknowledgments

We thank Dr. Petri Räisänen for the incoming solar radiation computations and Dr. Tristan Quaife for the snow albedo computations.

8.3.6.2 Forests, Aerosols and Climate Change

Ilona Riipinen, Tuukka Petäjä, Pertti Hari, Miikka dal Maso, Jaana Bäck, and Markku Kulmala

The Role of Aerosols in the Atmosphere

Generally, an aerosol is defined as a mixture of a carrier gas and solid or liquid particles suspended in it. In the case of atmospheric aerosols, the carrier gas is air, and the term 'atmospheric aerosol' refers to the mixture of air and *aerosol particles* suspended in the air. When we speak of aerosol concentrations, we refer to the amount (number, surface area or volume/mass) of suspended particles per some unit of carrier gas, usually a volume (like 1 cm^3) of air at atmospheric pressure.

For a particle to be considered an aerosol particle, it needs to remain suspended in air for a significant time. This basically defines a limit for the size of aerosol particles, as larger particles tend to fall to the ground by the pull of gravity. An upper limit for the size can be considered to be a few millimetres, the size of raindrops. Usually, the discussion of aerosol particles is limited to particle sizes smaller than about 100 μm (μm, one millionth of a metre). The lower boundary for the size of aerosol particles is in practise defined by the requirement of a liquid or solid phase (see, e.g. Vehkamaki 2006) and is typically around 1 nm in atmospheric conditions.

Atmospheric aerosols affect the climate in two distinct ways. First, they affect the Earth's radiation budget directly by scattering the solar radiation (direct effect). Second, they act as condensation nuclei for cloud droplets (CCN) having therefore a significant impact on the radiative properties and lifetimes of clouds (indirect aerosol effect). According to the latest report by the Intergovernmental Panel on Climate Change (IPCC 2007), the total climatic effect of atmospheric aerosols is estimated to be cooling: the radiative forcing resulting from the direct effect is estimated to be between −0.1 and −0.9 W m^{-2}, whereas the corresponding estimate for the indirect effect is −1.8 … –0.3 W m^{-2}. However, the IPCC also reports that the radiative forcing of the aerosols is currently subject to the largest uncertainties of all individual components in their radiative forcing calculations.

I. Riipinen (✉)
Department of Applied Environmental Science & Bert Bolin Center for Climate Research, Stockholm University, Stockholm, Sweden
e-mail: ilona.riipinen@itm.su.se

In this work, we provide rough estimates on how an increased aerosol number concentration resulting from increased biogenic activity would affect the aerosol radiative forcing.

According to recent global model calculations by Spracklen et al. (2006), approximately 30% of the global particle concentration originates from biogenic secondary aerosol formation events. However, the newly formed particles need to grow fast enough to survive to sizes (ca. 50–100 nm in diameter) at which they can act as cloud condensation nuclei and have a significant climatic effect—otherwise these small particles will be lost by coagulation and deposition processes (see, e.g. Kerminen and Kulmala 2002). Competition between the growth and loss processes is therefore among the main factors determining the magnitude of the particle source provided by the boreal forests.

Aerosol Formation and Growth

Based on their source, atmospheric aerosol particles can be roughly divided into primary and secondary particles. Primary particles, such as dust, sea salt or pollen, enter the atmosphere in the condensed (liquid or solid) phase, whereas secondary particles have been formed from condensable atmospheric vapours. This secondary formation of stable nanosised particles by condensation of gaseous matter is an important source of atmospheric aerosol particles. Such formation often occurs in bursts, called nucleation events, in which new small (a few nanometres in diameter) particles appear and grow to sizes large enough to have climatic importance. Nucleation events have been observed in several different environments around the world, and boreal forests have proven to be an important source of such secondary aerosol particles (see, e.g. Mäkelä et al. 1997; Kulmala et al. 2001, 2004a; Tunved et al. 2006).

An example of a particle formation event taking place at the SMEAR II station in Hyytiälä is shown in Fig. 8.33 (Mäkelä et al. 2000). A basic feature of a particle formation event is an increase in particle number, especially in the smallest observable sizes (3–25 nm). The formed particles then grow for several hours until they have reached sizes of 50–100 nm, where they can act as condensation nuclei for cloud droplets and therefore have a climatic effect. During growth, a part of the freshly formed particles coagulate (i.e. collide and stick) with pre-existing particles, and their number is therefore reduced. The time evolution of the particle size distribution can be obtained by considering the sources and sinks that different dynamical processes provide for the distribution (see, e.g. Seinfeld and Pandis 1998, and Chap. 2).

Atmospheric Aerosol Concentrations

Aerosols absorb, emit and reflect solar radiation as well as thermal radiation of the globe (Sect. 8.3.1). In this way, they contribute to the behaviour of the atmosphere and to the radiation available for photosynthesis. The biogenic volatile organic

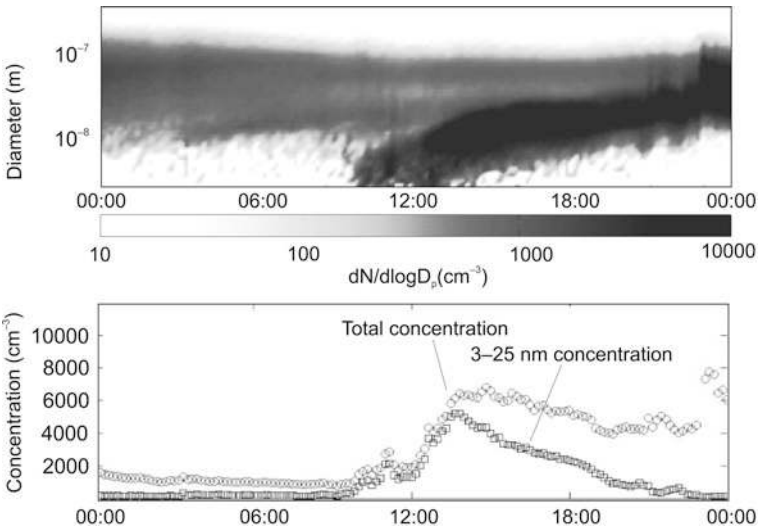

Fig. 8.33 Measured aerosol size distribution data during a particle formation event day. The upper panel shows the time evolution of the particle size distribution, with time on the horizontal axis and particle size on the vertical axis. The colour depicts particle concentrations; the darker the colour, the more particles of that size were observed. The lower panel shows the evolution of the total number concentration (*circles*) and the concentration of the smallest particles (*squares*). One can see that the increase of the particle number is almost exclusively due to formation of the very smallest particles; later, when the particles grow, the small particle number falls below the total number

compounds, BVOCs, emitted by vegetation, effect on the aerosol particle formation and growth. The BVOC emissions react to the climate change, and their contribution to aerosol dynamics will change. Thus, understanding of the formation and growth of aerosol particles is important for the analysis of feedbacks from boreal forests to climate change.

Taking a closer look at the times of particle formation in boreal forest, some clear patterns can be found. The bursts are almost exclusively observed during daytime, at least 2 h after sunrise and on average 3–4 h after sunrise but mostly before noontime. The start time of the bursts typically follows the variation of the time of sunrise (Mäkelä et al. 2000). Incoming solar radiation is found to correlate with the growth rate of the new particles, which leads to speculation that increasing amounts of radiation increase the photochemical production rate of condensing vapour, which increases the formation and growth rates of the particles. These effects naturally increase the probability of particles surviving the early stages of growth until they are detectable.

Probable compounds participating in the atmospheric nucleation are, for example, sulphuric acid, water, ammonia, amines and a variety of organic compounds. In boreal forest, the effect of the organics is clearly seen and a significant part of the condensing vapours is thought to be a mixture of oxidation products of volatile organic compounds (BVOC), which are emitted by trees (e.g. Hakola et al. 2003).

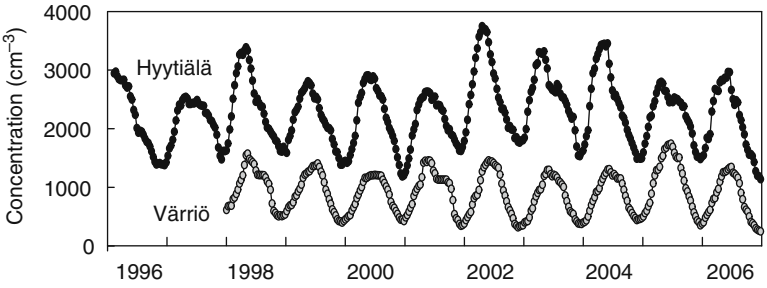

Fig. 8.34 The 4-month running average of the total particle concentration at SMEAR II, southern Finland (Hyytiälä) and at SMEAR I, northern Finland (Värriö). One can easily see the annual variation, with maxima in the summer and minima in the winter. The concentrations are clearly lower at SMEAR I than at SMEAR II

The exact role of condensable organics is not completely understood, but there are clear indications that organics are needed to explain the particle growth rates observed in the boreal forest (Kulmala et al. 2004b). Organics may also affect the very first steps of aerosol formation. However, exact information on, for example, the composition of the smallest atmospheric particles (1–10 nm in diameter) is very difficult to obtain with current commercial instruments.

The condensing vapours affect the aerosol climatic properties in several ways. By making the small particles grow, they increase the atmospheric lifetime of those particles and cause them to reach sizes at which they can act as cloud condensation nuclei. The vapours also naturally affect the composition and therefore the chemical and physical properties of the particles. As the particles deposit on the surfaces, they carry their constituents along with them. Therefore, depositing aerosol particles are also likely to contribute significantly to, for example, the nitrogen deposition.

Total fine particle number concentrations observed in the boreal forests typically range from 10 to 100,000 cm^{-3}, depending on the site, for instance, its distance from roads, cities and other sources of anthropogenic pollution. Figure 8.34 shows an exemplary time series of running 4-month averages of aerosol particle concentrations in the size range of 3–800 nm measured in 1996–2007 at the SMEAR II. The same figure presents also a similar plot for the years 1998–2007 in the cleaner environment of SMEAR I in Värriö. At remote continental sites like Hyytiälä and Värriö most of the particles are typically concentrated in the size range of ca. 50–150 nm. On average, approximately 30% of these, potentially climatically active, particles were originally formed in a nucleation event.

An exemplary plot on the seasonal variation of particle number concentrations in boreal forest is shown in Fig. 8.35, where the 2-week average particle concentration observed at SMEAR II during the year 2000 is plotted. In springtime, a clear maximum in the particle number concentration is observed, and a second, somewhat smaller, maximum is seen in the autumn. The daily variations of particle numbers on a day with clear nucleation and on the other hand on a non-event day are presented in Fig. 8.36. A clear increase in particle concentrations can be observed during new particle formation, compared to a day with no nucleation and growth.

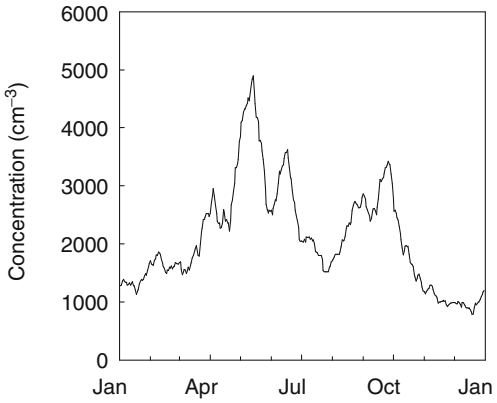

Fig. 8.35 The 2-week running average of the total particle number concentration at SMEAR II, southern Finland, in the year 2000. There is a seasonal variation with maxima in spring and autumn and minima in summer and winter

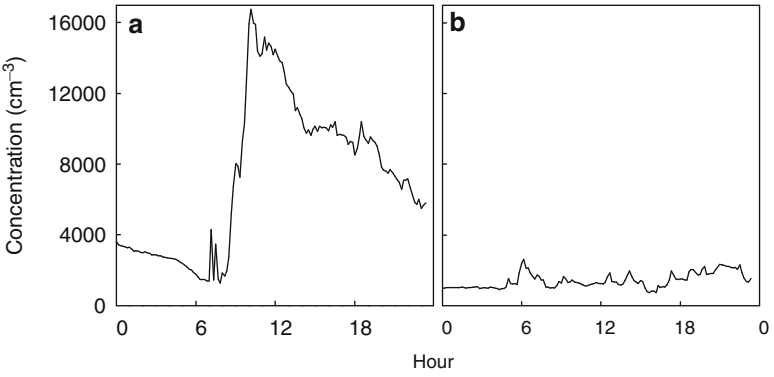

Fig. 8.36 The total particle number concentration during an event day (**a**) a non-event day (**b**) at SMEAR II, southern Finland. During the particle formation period (at ca. 10–11 o'clock) on an event day, the total particle number increases almost 10-fold. The particle number concentration fluctuates around a few thousand particles per cubic centimetre

The vertical profiles of the particle number concentrations vary as a function of, for example, the height of the mixed boundary layer, and the intensity of the possible nucleation in different parts of the troposphere. Figure 8.37 present a vertical concentration profile measured near the SMEAR II station on 3 March 2006 and 13 March 2006 (Laakso et al. 2007). The measurements were taken from a hot air balloon (Fig. 8.38) due to its high lifting capacity and capability to follow air mass. The first of the days shown here corresponds to a day without new particle formation, whereas the latter is a day with a clear nucleation event. The profiles reveal that during new particle formation the particles are clearly concentrated near the surface, whereas on the non-event day no such clear dependence on the measurement height is observed. This indicates that most observed nucleation takes place in the atmospheric boundary layer near the forest canopy, rather than at the

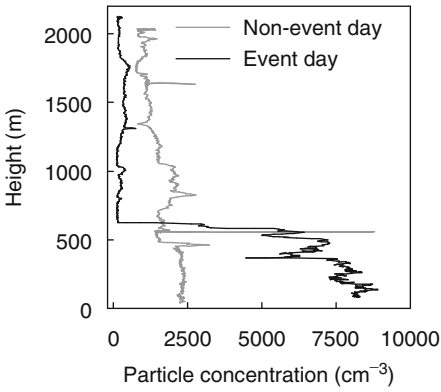

Fig. 8.37 The number concentration of over 10-nm particles as a function of altitude during a non-event day on 3 March 2006 and on an event day on 13 March 2006 at SMEAR II, southern Finland. No significant altitude dependence is observed on the non-event day. The particle number concentration has a clear maximum close to the Earth's surface on the event day

Fig. 8.38 Hot air balloon taking off with eager researchers for boundary-layer profile measurements. The wooden buildings are the dormitory for students and old dining room at Hyytiälä

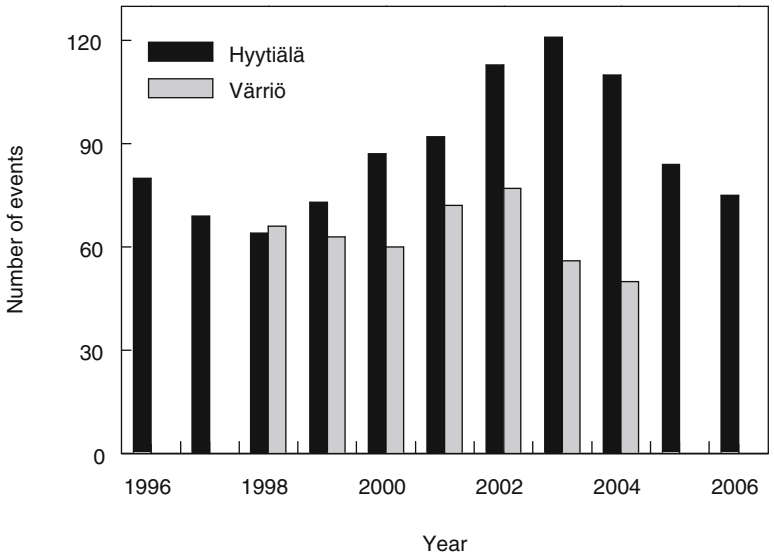

Fig. 8.39 The number of particle formation events at SMEAR I, northern Finland (Värriö) in 1998–2004 and SMEAR II, southern Finland (Hyytiälä) in 1996–2006

higher altitudes. This observation supports the idea that compounds emitted by forest vegetation have an important role in new particle formation, and particularly in particle growth

Annual Cycle of Nucleation Events

Classification and selection of event and non-event days reveals that tropospheric particle formation in the boreal forest is quite common, at least more common than previously assumed. In Hyytiälä, roughly every fourth day is found to contain a particle formation burst, based on the analysis of the particle size distribution data from years 1996 to 2006 (Dal Maso et al. 2005, 2007). For SMEAR I in Värriö, the corresponding frequency is one event every 5 days (Dal Maso et al. 2007). The annual statistics of nucleation event days for Hyytiälä in 1996–2006 and Värriö in 1996–2004 are presented in Fig. 8.39.

On the seasonal scale, two clear peaks in formation frequency are found: one in springtime (March–May) and another centred around September. During these periods, the event fraction in Hyytiälä is typically over 50% of all days and even higher than that if undefined days are removed from the statistics. In contrast, wintertime (November to mid-February) is a very inactive time for particle formation. In summer, a dip in the frequency is observed. The annual distribution of nucleation event days in the more northern Värriö station is similar, with a somewhat less clear minimum in the summer. Summaries of the annual variation of the occurrence of

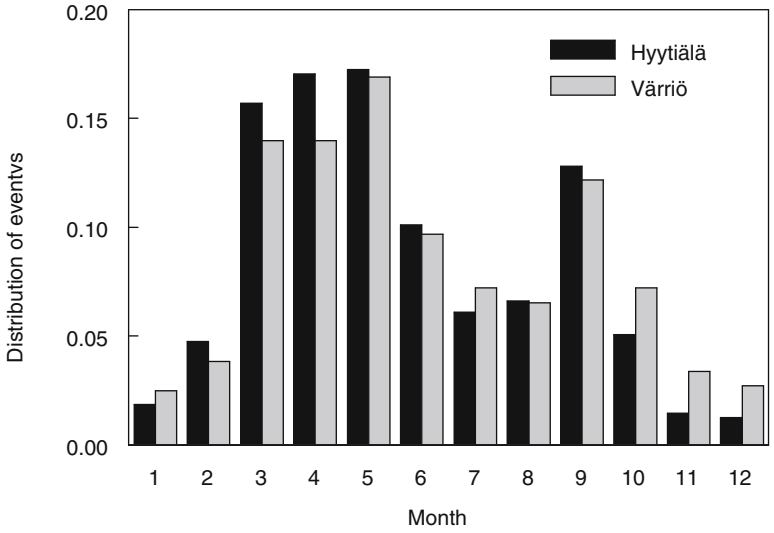

Fig. 8.40 The monthly distribution of particle formation events at SMEAR I and SMEAR II, northern and southern Finland

nucleation events for Hyytiälä and Värriö are presented in Fig. 8.40. The springtime peaks in particle formation are related to the spring recovery of photosynthesis (Sect. 4.2.2), the forest vegetation and related emissions of biogenic organics.

BVOC Emissions Under Changing Climate

The group of the biogenic volatile organic compounds (BVOCs) in the atmosphere-plant interface is very heterogeneous, both in respect of their chemical properties such as volatility and hydrophobicity and in respect of their biogenic origin. The BVOCs are emitted from vegetation as mixtures of compounds, and these mixtures change in time both seasonally and diurnally. BVOCs can be synthesised in both aerial and below-ground plant parts, in floral, vegetative and structural tissues, and they are stored in significant quantities in many plant genera. Their emissions show a conspicuous and compound-specific seasonal pattern. For most compounds, the emission rates are highest in summer and lower, although still significant, in spring and autumn. Even during wintertime, emissions of some BVOCs can be measured (Tarvainen et al. 2005; Hakola et al. 2006).

BVOCs are not found uniformly within the plant. The constituent, defence-related compounds are often located in conifers in resin ducts of needles and resin canals in their trunks. From there, they can be liberated if necessary for defence purposes, for example, after a pathogen or herbivore attack. Another, temporally more fluctuating group of BVOCs is located in, for example, air spaces of photosynthesising tissues and is readily diffused to the boundary layer and further to the atmosphere.

The synthesis of monoterpenes occurs in mesophyll chloroplasts, and the recently synthesised monoterpenes are temporarily located in liquid phase in the apoplast. From the liquid phase, they diffuse to the leaf surface and are emitted into the atmosphere. It is assumed that two independent processes influence emissions from needles to the atmosphere: one is biosynthesis, related to the instantaneous irradiation and mesophyll CO_2 concentration, and the other is temperature-dependent emission from pools. The monoterpene emission processes from Scots pine needles include substrate production, monoterpene biosynthesis, storage, transport within the leaf, and finally emission.

Effects of climate change on ecosystem-level BVOC emissions are produced by many, partially opposite, responses to changing factors, which makes evaluating the net effects at the ecosystem level very difficult (see, e.g. Penuelas and Staudt 2010).

Rising temperatures enhance enzyme activity and accelerate diffusion of BVOCs and thereby increase their volatilisation from tissues. Warming also leads to prolonged growing season and thus longer duration of high emission rates from leafy tissues especially from deciduous trees which normally are considered to be high emitters. Mild drought is reported to increase BVOC emissions, whereas severe drought might result in opposite effects due to substrate or enzyme limitations. Since BVOC biosynthesis is strongly limited by carbon availability, good correlations with photosynthetic rates have been found in many species. The majority of studies report increases in BVOC emissions after N fertilisation or a positive correlation with foliar N levels.

However, short-term exposures to elevated CO_2 often reduce leaf-level isoprenoid emissions, whereas growth in subambient CO_2 tends to increase emissions. Under elevated CO_2, the correlations between the measured emissions and both leaf temperatures and photosynthetic rates become more vague. Emission reductions due to elevated CO_2 have been connected with metabolic competition for intermediates, or downregulation due to lack of energy supply (e.g. Rosenstiel et al. 2003). The instantaneous emission responses may differ from long-term responses at elevated CO_2, and therefore, predictions on emission rates for a time period of years to decades, which are based on short-term experiments, are very problematic (e.g. Niinemets et al. 2010).

We assume that increasing temperature and atmospheric CO_2 concentration accelerates photosynthesis, thus producing more substrates for isoprenoid biosynthesis, and therefore the BVOC emissions increase proportionally to the increase in photosynthesis. Also direct effects of temperature rise to the volatilisation of BVOCs increase their emissions. This assumed behaviour is not in conflict, although not strongly supported by the present experimental results either since the mechanisms of CO_2 influence on BVOC biosynthesis are still ambiguous.

Increasing atmospheric CO_2 concentration accelerates photosynthesis, and the relationship is nearly linear at present atmospheric concentration (Sect. 4.2.2). The acclimation of photosynthesis to changing CO_2 concentration cannot be predicted since it has not been tested in evolution, at least during the last million years. In addition, the increase in needle mass, caused by accelerated decomposition of proteins due to temperature increase, will still enhance the photosynthesis of boreal forests.

Despite of insufficient understanding of the BVOC emission responses to climate change, we know that the synthesis of many compounds is closely linked with photosynthesis at present concentration ranges. Enhanced photosynthetic production, in connection with increasing leaf biomass will strongly influence the BVOC emissions from boreal forest stands in the future climate. Positive effects on emissions are also expected to follow from changes in water and nutrient availability, and increased temperature, in particular for those compounds that are having permanent storage pools in the foliage and trunks, such as monoterpenes. Taking these factors into account, we can roughly assume that the response of BVOC emissions to climatic change is resembling that of photosynthesis.

The photosynthetic production was doubled in simulations with MicroForest at the year 2100. This is why we assume that the BVOC emissions will also double in the year 2100 when compared with present emissions. However, we realise that this is an assumption where potential significant interactions, for example, increased respiratory demands for substrates involved in BVOC biosynthesis (Rosenstiel et al. 2003), may partially cancel the effects of increased photosynthetic production on emissions. In the future, when more field measurements will be available for testing and developing of knowledge, the present emission approximation should be improved.

Climatic Effects of Increasing Aerosols Due to BVOC Emissions from Forests

Condensable vapour concentration affects aerosol particle formation and growth. Anthropogenic emissions of CO_2 change the atmospheric CO_2 concentration, accelerate photosynthesis and consequently potentially also BVOC emissions from boreal forests. The emitted volatile carbon compounds react in the air and lose their volatility and condense to form and grow aerosol particles. Thus, changes in boreal forests influence the aerosols in the air.

Condensation of the oxidation products of volatile organic compounds (BVOCs) emitted by boreal forests seems to explain a significant fraction of the observed 3–25-nm particle growth rates at the SMEAR I and II sites (Kulmala et al. 1998, 2004a; Hirsikko et al. 2005). Besides their evident role in particle growth above 3 nm, it is possible that the organics emitted by the forests affect also the very first steps of the particle formation and growth processes. The atmospheric particle formation takes place close to 2 nm in diameter and the growth rates observed for the 2–3 nm particles (ca. $1.5\,\mathrm{nm\,h^{-1}}$, see, e.g. Hirsikko et al. 2005) are typically approximately half of the values reported for particles larger than 3 nm (ca. $3\,\mathrm{nm\,h^{-1}}$, e.g. Dal Maso et al. 2005).

Because of the links between the BVOCs and the particle formation, an increase in BVOC emissions is likely to result in an increase of the particle source provided by the boreal forests (see also Kulmala et al. 2004c). The change in the produced climatically active aerosol particle number will affect the climatic role of boreal forests: an increase in the cloud condensation nuclei number would lead to more

long-lived clouds and therefore add to a negative feedback between climate warming and particle production (IPCC 2007).

To assess this feedback between climate change and boreal forests, we have made rough estimates on the increase of the production of 150-nm particles resulting from doubling the emissions of BVOCs. We assumed that the particle formation rate at 2 nm (J_2) stays constant over time, being approximately 1 cm^{-3} s^{-1}. We then calculated the corresponding formation rates at 3 and 150 nm (J_3 and J_{150}) now and in the future when BVOC emissions are doubled compared to the current situation. The calculations were made taking into account an increase of growth rates caused by an increasing amount of BVOCs, and their effect on the competition of growth and coagulation losses (see Kerminen and Kulmala 2002 for details).

In the estimations, the growth rate of 2–3-nm particles was assumed to be 1.5 nm^{-1}, and the growth rate of particles larger than 3 nm was set to 3 nm^{-1}. We first assumed that the organics start to contribute to growth from the very beginning, that is, from 2 nm, and second that they start to condense on the particles only when they have reached sizes above 3 nm, the latter being the more likely case. The ratios of the 150-nm particle production rates in the future (with doubled BVOC emissions) and at the present time are 130–300% in the case when organics contribute in the growth from 2 nm and 103–110% in the case when the organics contribute to the growth from 3 nm. The obtained ratio in the 150-nm particle production rates ranges from 103 to 300%, which would enhance the climate cooling effect of the forest-produced aerosol at least with the same factor compared to the current radiative forcing (estimated to be between −0.03 and −1.1 W m^{-2}; see Kurtén et al. 2003). However, the response between the aerosol source strength and the radiative transfer is highly nonlinear, so these estimations are subject to significant uncertainties and should be treated as order of magnitude estimations only.

The predicted changes in emissions of volatile organic compounds from forests in response to climate change will increase aerosol formation in these areas. This phenomenon is rather weakly known, and thus, the aerosols increase uncertainty in the expected climate change.

References

Andreae MO, Jones CD, Cox PM (2005) Strong present-day aerosol cooling implies a hot future. Nature 435:1187–1190

Arya SP (2001) Introduction to micrometeorology, 2nd edn. Academic, London

BACC Author Team (2008) Assessment of climate change for the Baltic Sea basin, regional climate studies. Springer, Heidelberg

Barnola J-M, Raynaud D, Lorius C, Barkov NI (2003) Historical CO_2 record from the Vostok ice core. In: Boden TA et al (eds) Trends: a compendium of data on global change. Carbon Dioxide Information Analysis Center, Oak Ridge National Laboratory, U.S. Department of Energy, Oak Ridge

Betts RA, Falloon PD, Goldewijk KK, Ramankutty N (2007) Biogeophysical effects of land use on climate: model simulations of radiative forcing and large-scale temperature change. Agric For Meteorol 142:216–233

Bird RB, Stewart WE, Lightfoot EN (2002) Transport phenomena, 2nd edn. Wiley, New York
Boer GJ, Yu B (2003) Climate sensitivity and response. Clim Dyn 20:415–429
Bonan GB, Pollard D, Thompson SL (1992) Effects of boreal forest vegetation on global climate. Nature 359:716–718
Botkin DB, Simpson L (1990) The first statistically valid estimate of biomass for a large region. Biogeochemistry 9:161–174
Chen JM, Black TA (1992) Defining leaf area index for non-flat leaves. Plant Cell Environ 15:421–429
Colman R (2003) A comparison of climate feedbacks in general circulation models. Clim Dyn 20:865–873
Cox PM, Betts RA, Jones CD, Spall SA, Totterdell IJ (2000) Acceleration of global warming due to carbon-cycle feedbacks in a coupled climate model. Nature 408:184–187
Dai A, Trenberth KE, Qian T (2004) A global data set of Palmer Drought Severity Index for 1870–2002: relationship with soil moisture and effects of surface warming. J Hydrometeorol 5:1117–1130
Dal Maso M, Kulmala M, Riipinen I, Wagner R, Hussein T, Aalto PP, Lehtinen KEJ (2005) Formation and growth of fresh atmospheric aerosols: eight years of size distribution data from SMEAR II, Hyytiälä, Finland. Boreal Environ Res 10:323–336
Dal Maso M, Sogacheva L, Aalto PP, Riipinen I, Komppula M, Tunved P, Korhonen L, Suur-Uski V, Hirsikko A, Kurtén T, Kerminen V-M, Lihavainen H, Viisanen Y, Hansson H-C, Kulmala M (2007) Aerosol size distribution measurements at four Nordic field stations: identification, analysis and trajectory analysis of new particle formation bursts. Tellus B59:350–361
Dawson TP, Curran PJ, Plummer SE (1998) LIBERTY—modelling the effects of leaf biochemical concentration on reflectance spectra. Remote Sens Environ 65:50–60
Dentener F (2006) Global maps of atmospheric nitrogen deposition, 1860, 1993, and 2050. Data set from Oak Ridge National Laboratory, Oak Ridge, Tennessee. http://www.daac.ornl.gov/
Ebermayer E (1876) Die gesamte Lehre von der Waldstreu. Springer, Berlin
Eriksson H, Karlsson K (1997) Olika gallrings och gödslingsregimens effekter på beståndsut vecklingen baserat på långliggande experiment i tall-och granbestånd i Sverige. SLU, Inst Skogsprodukt Rep 42:1–135
Forster P, Ramaswamy V, Artaxo P, Berntsen T, Betts RA, Fahey DW, Haywood J, Lean J, Lowe DC, Myhre G, Nganga J, Prinn R, Raga G, Schulz M, van Dorland R (2007) Changes in atmospheric constituents and in radiative forcing. In: Solomon S, Qin D, Manning M, Chen Z, Marquis M, Averyt KB, Tignor M, Miller HL (eds) Climate change 2007: the physical science basis. Cambridge University Press, Cambridge
Friedli H, Lötscher H, Oeschger H, Siegenthaler U, Stauffer B (1986) Ice core record of $^{13}C/^{12}C$ ratio of atmospheric CO_2 in the past two centuries. Nature 324:237–238
Freidenreich SM, Ramaswamy V (1999) A new multiple-band solar radiative parameterization for general circulation models. J Geophys Res 104:31389–31409
Friedlingstein P, Cox P, Betts R et al (2006) Climate-carbon cycle feedback analysis: results from the C4MIP model intercomparison. J Clim 19:3337–3353
Gauthier S, Bergman A, Bergeron Y (1996) Forest dynamics modelling under natural fire cycles: a tool to define natural mosaic diversity for forest management. Environ Monit Assess 39:417–434
Groisman PY, Sherstyukov BG, Razuvaev VN, Knight RW, Enloe JG, Stroumentova NS, Whitfield PH, Førland E, Hannsen-Bauer I, Tuomenvirta H, Alexandersson H, Mescherskaya AV, Karl TR (2007) Potential forest fire danger over Northern Eurasia: changes during the 20th century. Glob Planet Change 56:371–386
Hagemann S (2002) An improved land surface parameter data set for global and regional climate models. Max-Planck-Institute for Meteorology, Report 336. Hamburg, Germany
Hakola H, Laurila T, Hiltunen V, Hellen H, Keronen P (2003) Seasonal variation of VOC concentrations above a boreal coniferous forest. Atmos Environ 37:1623–1634
Hakola H, Tarvainen V, Bäck J, Ranta H, Bonn B, Rinne J, Kulmala M (2006) Seasonal variation of mono- and sesquiterpene emission rates of Scots pine. Biogeosciences 3:93–101

Hansen J, Lacis A, Rind D, Russell G, Stone P, Fung I, Ruedy R, Lerner J (1984) Climate sensitivity: analysis of feedback mechanisms. Meteorol Monogr 29:130–163

Hansen J, Sato M, Ruedy R et al (2005) Efficacy of climate forcings. J Geophys Res 110:D18104

Harvey LDD (2000) Global warming: the hard science. Pearson Education, Harlow

Hegerl GC, Zwiers FW, Braconnot P, Gillett NP, Luo Y, Marengo J, Nicholls N, Penner JE, Stott PA (2007) Understanding and attributing climate change. In: Solomon S, Qin D, Manning M, Chen Z, Marquis M, Averyt KB, Tignor M, Miller HL (eds) Climate change 2007: the physical science basis. Cambridge University Press, Cambridge

Held IM, Soden BJ (2006) Robust responses of the hydrological cycle to global warming. J Clim 19:5686–5699

Helmisaari H-S, Holt Hanssen K, Jacobson S, Kukkola M, Luiro J, Saarsalmi A, Tamminen P, Tveite B (2011) Logging residue removal after thinning in Nordic boreal forests: long-term impact on tree growth. For Ecol Manag 261:1919–1927

Hirsikko A, Laakso L, Hõrrak U, Aalto PP, Kerminen V-M, Kulmala M (2005) Annual and size dependent variation of growth rates and ion concentrations in boreal forest. Boreal Environ Res 10:357–370

Holton JR (2004) An introduction to dynamic meteorology. Elsevier Academic Press, New York

Houghton J (2004) Global warming: the complete briefing. Cambridge University Press, Cambridge, UK

Houghton JT, Ding Y, Griggs DJ, Noguer M, van der Linden PJ, Xiaosu D (eds) (2001) Climate Change 2001. The scientific basis. Contribution of working group I to the third assessment report of the Intergovernmental Panel on Climate Change (IPCC). Cambridge University Press, Cambridge

Huntington TG (2006) Evidence for intensification of the global water cycle: review and synthesis. J Hydrol 319:83–95

Hyytiäinen K, Tahvonen O, Valsta L (2005) Optimum juvenile density, harvesting, and stand structure in even-aged Scots pine stands. For Sci 51:120–133

IPCC (2007) Contribution of working group I to the fourth assessment report of the Intergovernmental Panel on Climate Change. In: Solomon S, Qin D, Manning M, Chen Z, Marquis M, Averyt K, Tignor MMB, Miller HL (eds) Climate change 2007: the physical science basis. Cambridge University Press, Cambridge

Jansen E, Overpeck J, Briffa KR et al (2007) Paleoclimate. In: Solomon S, Qin D, Manning M, Chen Z, Marquis M, Averyt KB, Tignor M, Miller HL (eds) Climate Change 2007: the physical science basis. Contribution of working group I to the fourth assessment report of the Intergovernmental Panel on Climate Change (IPCC). Cambridge University Press, Cambridge

Jin M, Liang S (2006) An improved land surface emissivity parameter for land surface models using global remote sensing observations. J Clim 19:2867–2881

Jones PD, Lister DH (2002) The daily temperature record for St. Petersburg (1743–1996). Clim Chang 53:253–267

Joshi M, Shine K, Ponater M, Stuber N, Sausen R, Li L (2003) A comparison of climate response to different radiative forcings in three general circulation models: towards an improved metric of climate change. Clim Dyn 20:843–854

Jouzel J, Lorius C, Petit JR, Genthon C, Barkov NI, Kotlyakov VM, Petrov VM (1987) Vostok ice core: a continuous isotope temperature record over the last climatic cycle (160,000 years). Nature 329:403–408

Jouzel J, Barkov NI, Barnola JM, Bender M, Chappellaz J, Genthon C, Kotlyakov VM, Lipenkov V, Lorius C, Petit JR, Raynaud D, Raisbeck G, Ritz C, Sowers T, Stievenard M, Yiou F, Yiou P (1993) Extending the Vostok ice-core record of palaeoclimate to the penultimate glacial period. Nature 364:407–412

Jouzel J, Waelbroeck C, Malaize B, Bender M, Petit JR, Stievenard M, Barkov NI, Barnola JM, King T, Kotlyakov VM, Lipenkov V, Lorius C, Raynaud D, Ritz C, Sowers T (1996) Climatic interpretation of the recently extended Vostok ice records. Clim Dyn 12:513–521

Keeling CD, Whorf TP (2005) Atmospheric CO_2 records from sites in the SIO air sampling network. In: Boden TA et al (eds) Trends: a compendium of data on global change. Carbon

Dioxide Information Analysis Center, Oak Ridge National Laboratory, U.S. Department of Energy, Oak Ridge

Kerminen V-M, Kulmala M (2002) Analytical formulae connecting the "real" and the "apparent" nucleation rate and the nuclei number concentration for atmospheric nucleation events. J Aerosol Sci 33:609–622

Kiehl JT, Trenberth KE (1997) Earth's annual global mean energy budget. Bull Amer Meteor Soc 78:197–208

Kulmala M, Toivonen A, Mäkelä JM, Laaksonen A (1998) Analysis of the growth of nucleation mode particles observed in Boreal forest. Tellus 50B:449–463

Kulmala M, Dal Maso M, Mäkelä JM, Pirjola L, Väkevä M, Aalto P, Miikkulainen P, Hämeri K, O'Dowd CD (2001) On the formation, growth and composition of nucleation mode particles. Tellus 53B:479–490

Kulmala M, Vehkamäki H, Petäjä T, Dal Maso M, Lauri A, Kerminen V-M, Birmili W, McMurry PH (2004a) Formation and growth rates of ultrafine atmospheric particles: a review of observations. J Aerosol Sci 35:143–176

Kulmala M, Laakso L, Lehtinen KEJ, Riipinen I, Dal Maso M, Anttila T, Kerminen V-M, Hõrrak U, Vana M, Tammet H (2004b) Initial steps of aerosol growth. Atmos Chem Phys 4:2553–2560

Kulmala M, Suni T, Lehtinen KEJ, Dal Maso M, Boy M, Reissell A, Rannik Ü, Aalto PP, Keronen P, Hakola H, Bäck J, Hoffmann T, Vesala T, Hari P (2004c) A new feedback mechanism linking forests, aerosols, and climate. Atmos Chem Phys 4:557–562

Kurtén T, Kulmala M, Dal Maso M, Suni T, Reissell A, Vehkamäki H, Hari P, Laaksonen A, Viisanen Y, Vesala T (2003) Estimation of different forest-related contributions to the radiative balance using observations in southern Finland. Boreal Environ Res 8:275–285

Laakso L, Grönholm T, Kulmala L, Haapanala S, Hirsikko A, Lovejoy ER, Kazil J, Kurtén T, Boy M, Nilsson ED, Sogachev A, Riipinen I, Stratmann F, Kulmala M (2007) Hot-air balloon as a platform for boundary layer profile measurements during particle formation. Boreal Env Res 12:279–294

Lemke P, Ren J, Alley R, Allison I, Carrasco J, Flato G, Fuiji Y, Kaser G, Mote P, Thomas R, Zhang T (2007a) Observations: changes in snow, ice and frozen ground. In: Solomon S, Qin D, Manning M, Chen Z, Marquis M, Averyt KB, Tignor M, Miller HL (eds) Climate Change 2007: the physical science basis. Contribution of Working Group I to the Fourth Assessment Report of the Intergovernmental Panel on Climate Change. Cambridge University Press, Cambridge

Lemke P, Ren J, Alley R, Allison I, Carrasco J, Flato G, Fuiji Y, Kaser G, Mote P, Thomas R, Zhang T (2007b) Observations: changes in snow, ice and frozen ground. In: Solomon S, Qin D, Manning M, Chen Z, Marquis M, Averyt KB, Tignor M, Miller HL (eds) Climate Change 2007: the physical science basis. Contribution of working group I to the fourth assessment report of the Intergovernmental Panel on Climate Change (IPCC). Cambridge University Press, Cambridge

Magnani F, Mencuccini M, Borghetti M, Berbigier P, Berninger F, Delzon S, Grelle A, Hari P, Jarvis PG, Kolari P, Kowalski AS, Lankreijer H, Law BE, Lindroth A, Loustau D, Manca G, Moncrieff JB, Rayment M, Tedeschi V, Valentini R, Grace J (2007) The human footprint in the carbon cycle of temperate and boreal forests. Nature 447:848–850

Mäkelä JM, Aalto P, Jokinen V, Pohja T, Nissinen A, Palmroth S, Markkanen T, Seitsonen K, Lihavainen H, Kulmala M (1997) Observations of ultrafine aerosol formation and growth in boreal forest. Geophys Res Lett 24:1219–1222

Mäkelä JM, Dal Maso M, Pirjola L, Keronen P, Laakso L, Kulmala M, Laaksonen A (2000) Characteristics of the atmospheric particle formation events observed at a boreal forest site in southern Finland. Boreal Environ Res 5:299–313

McClatchey RA, Fenn RW, Selby JEA, Volz FE, Garing JS (1971) Optical properties of the atmosphere. Report AFCRL-71-0279. Air Force Geophys Lab, Hanscom Air Force Base, Bedford

Meehl GA, Stocker TF, Collins W, Friedlingstein P, Gaye A, Gregory J, Kitoh A, Knutti R, Murphy J, Noda A, Raper S, Watterson I, Weaver A, Zhao Z-C (2007) Global climate projections. In: Solomon S, Qin D, Manning M, Chen Z, Marquis M, Averyt KB, Tignor M,

Miller HL (eds) Climate Change 2007: the physical science basis. Contribution of working group I to the fourth assessment report of the Intergovernmental Panel on Climate Change (IPCC). Cambridge University Press, Cambridge

Moberg A, Bergström H, Krigsman JR, Svanered O (2002) Daily air temperature and pressure series for Stockholm (1756–1998). Clim Chang 53:171–212

Myneni RB, Dong J, Tucker CJ, Kaufmann RK, Kauppi PE, Liski J, Zhou L, Alexeyev V, Hughes MK (2001) A large carbon sink in the woody biomass of Northern forests. Proc Natl Acad Sci USA 98:14784–14789

Nakićenović N, Swart R (eds) (2000) Emissions scenarios. A special report of working group III of the Intergovernmental Panel on Climate Change. Cambridge University Press, Cambridge

Niinemets U, Arneth A, Kuhn U, Monson RK, Penuelas J, Staudt M (2010) The emission factor of volatile isoprenoids: stress, acclimation, and developmental responses. Biogeosciences 7:2203–2223

Niinimäki S, Tahvonen O, Mäkelä A (2012) Applying a process-based model in Norway spruce management. For Ecol Manag 265:102–115

Nobel PS (2005) Physicochemical & environmental plant physiology, 3rd edn. Academic Press/Elsevier, San Diego

Penuelas J, Staudt M (2010) BVOCs and global change. Trends Plant Sci 15:133–144

Peterson TC, Vose RS (1997) An overview of the Global Historical Climatology Network temperature database. Bull Am Meteorol Soc 78:2837–2848

Petit JR, Jouzel J, Raynaud D, Barkov NI, Barnola J-M, Basile I, Bender M, Chappellaz J, Davis M, Delayque G, Delmotte M, Kotlyakov VM, Legrand M, Lipenkov VY, Lorius C, Pepin L, Ritz C, Saltzman E, Stievenard M (1999) Climate and atmospheric history of the past 420,000 years from the Vostok ice core, Antarctica. Nature 399:429–436

Räisänen J (2007) How reliable are climate models? Tellus 59A:2–29

Roeckner E, Bäuml G, Bonaventura L, Brokopf R, Esch M, Giorgetta M, Hagemann S, Kirchner I, Kornbleuh L, Manzini E, Rhodin A, Schlese U, Schulzweida U, Tomkins A (2003) The atmospheric general circulation model ECHAM5, Part I: Model description. Max-Planck-Inst Meteorol Rep 349, Hamburg

Roeckner E, Brokopf R, Esch M, Giorgetta M, Hagemann S, Kornblueh L, Manzini E, Schlese U, Schulzweida U (2006) Sensitivity of simulated climate to horizontal and vertical resolution in the ECHAM5 atmosphere model. J Clim 19:3771–3791

Rosenstiel TN, Potosnak MJ, Griffin KL, Fall R, Monson R (2003) Increased CO2 uncouples growth from isoprene emission in an agriforest ecosystem. Nature 421:256–259

Ross J (1981) The radiation regime and architecture of plant stands. Kluwer Academic, The Hague

Sausen R, Barthel K, Hasselman K (1988) Coupled ocean–atmosphere models with flux-correction. Clim Dyn 2:145–163

Schultz MG et al (2007) Reanalysis of the tropospheric chemical composition of the past 40 years (RETRO)—a long-term global modelling study of tropospheric chemistry. Final Rep 48/2007, Max Planck Inst Meteorol, Hamburg

Seinfeld JH, Pandis SN (1998) Atmospheric chemistry and physics. Wiley, New York

Smith TM, Reynolds RW (2005) A global merged land and sea surface temperature reconstruction based on historical observations (1880–1997). J Clim 18:2021–2036

Smolander S, Stenberg P (2005) Simple parameterizations of the radiation budget of uniform broadleaved and coniferous canopies. Remote Sens Environ 94:355–363

Spracklen DV, Carslaw KS, Kulmala M, Kerminen V-M, Mann GW, Sihto S-L (2006) The contribution of boundary layer nucleation events to total particle concentrations on regional and global scales. Atmos Chem Phys 6:5631–5648

Stamnes K, Tsay SC, Wiscombe W, Jayaweera K (1988) A numerically stable algorithm for discrete-ordinate-method radiative transfer in multiple scattering and emitting layered media. Appl Optics 27:2502–2509

Stamnes K, Tsay SC, Wiscombe W, Laszlo I (2000) A general-purpose numerically stable computer code for discrete-ordinate-method radiative transfer in scattering and emitting layered media, DISORT Rep v1.1. Stevens Inst Tech, Hoboken

Stephens BB, Gurney K, Tans P, Sweeney C, Peters W, Bruhwiler L, Ciais P, Ramonet M, Bousquet P, Nakazawa T, Aoki S, Machida T, Inoue G, Vinnichenko N, Lloyd J, Jordan A, Heimann M, Shibistova O, Langenfelds RL, Steele LP, Francey RJ, Denning AS (2007) Weak northern and strong tropical land carbon uptake from vertical profiles of atmospheric CO_2. Science 316:1732–1735

Tarvainen V, Hakola H, Hellen H, Bäck J, Hari P, Kulmala M (2005) Temperature and light dependence of the VOC emissions of Scots pine. Atmos Chem Phys 5:6691–6718

Trenberth KE, Jones PD, Ambenje P, Bojariu R, Easterling D, Klein Tank A, Parker D, Rahimzadeh F, Renwick JA, Rusticucci M, Soden B, Zhai P (2007) Observations: surface and atmospheric climate change. In: Solomon S, Qin D, Manning M, Chen Z, Marquis M, Averyt KB, Tignor M, Miller HL (eds) Climate Change 2007: The physical science basis. Contribution of working group I to the fourth assessment report of the Intergovernmental Panel on Climate Change (IPCC). Cambridge University Press, Cambridge

Tunved P, Hansson H-C, Kerminen V-M, Ström J, Dal Maso M, Lihavainen H, Viisanen Y, Aalto PP, Komppula M, Kulmala M (2006) High natural aerosol loading over boreal forests. Science 312:261–263

van Aardenne JA, Dentener FJ, Olivier JGJ, Goldewijk K, Lelieveld J (2001) A 1 deg × 1 deg resolution dataset of historical anthropogenic trace gas emissions for the period 1890–1990. Glob Biogeochem Cycles 15:909–928

Vehkamaki H (2006) Classical nucleation theory in multicomponent systems. Springer, Berlin

Vesala T, Suni T, Rannik U, Keronen P, Markkanen T, Sevanto S, Grönholm T, Smolander S, Kulmala M, Ilvesniemi H, Ojansuu R, Uotila A, Levula J, Mäkelä A, Pumpanen J, Kolari P, Kulmala L, Altimir N, Berninger F, Nikinmaa E, Hari P (2005) Effect of thinning on surface fluxes in a boreal forest. Glob Biogeochem Cycles 19:GB2001

Webb MJ, Senior CA, Sexton DMH, Ingram WJ, Williams KD, Ringer MA, McAvaney BJ, Colman R, Soden BJ, Gudgel R, Knutson T, Emori S, Ogura T, Tsushima Y, Andronova N, Li B, Musat I, Bony S, Taylor KE (2006) On the contribution of local feedback mechanisms to the range of climate sensitivity in two GCM ensembles. Clim Dyn 27:17–38

Wohlfahrt J, Harrison SP, Braconnot P (2004) Synergistic feedbacks between ocean and vegetation on mid- and high-latitude climates during the mid-Holocene. Clim Dyn 22:223–238